Investigating the Functional Significance of O-GlcNAc Substrate/Interactor Networks

Thesis by

Rita Beth Aksenfeld

In Partial Fulfilment of the Requirements for the Degree of
BACHELOR OF SCIENCE IN CHEMISTRY

CALIFORNIA INSTITUTE OF TECHNOLOGY
Pasadena, California

2020
Defended June 5, 2020

Acknowledgements

First, I would like to thank my thesis advisor, Linda Hsieh-Wilson, for welcoming me into her group. The past two and a half years working in your lab have taught me so much and have been instrumental in my growth as a student and as a scientist. In your lab, I developed a passion for chemical biology and for academic research at the highest level. I am deeply grateful for your endless support and confidence in me.

To John Thompson, I cannot thank you enough for your mentorship throughout the years. You have been a great teacher, and your extraordinary dedication to science and to mentorship has been a constant source of inspiration as I navigate my own scientific path. Thank you for your patience in teaching me so many things about lab work and scientific writing, for answering all my questions, and for giving me my own project and encouraging my independence from an early stage. That has really made all the difference. Thank you again for being such a phenomenal mentor; I am honored to have been your student.

Finally, I'd like to thank everyone in the Hsieh-Wilson lab throughout the years for their support and advice throughout my time working with them. I especially want to thank my collaborators Matthew Griffin and Yao Xiao for the O-GlcNAc networks and Katsuya Colón for the image processing code.

This project was a collaboration, running titles:

1. Functional Glycoproteomics by Integrated Network Assembly and Partitioning. John W. Thompson,* Matthew E. Griffin,* Yao Xiao,* Michael J. Sweredoski, Rita B. Aksenfeld, Elizabeth H. Jensen, Yelena Koldobskaya, Andrew L. Schacht, Terry D. Kim, Priya Choudhry, Annie Moradian, Brett Lomenick, Spiros D. Garbis, Linda C. Hsieh-Wilson.

2. Quantitative Functional Glycoproteomics Reveals Widespread Changes in the db/db Mouse Liver. John W. Thompson,* Matthew E. Griffin,* Michael J. Sweredoski, Rita B. Aksenfeld, Daniel E. Mason, Annie Moradrian, Eric C. Peters, Linda C. Hsieh-Wilson.

*Denotes equal contribution.

Abstract

O-linked β-*N*-acetylglucosamine glycosylation (O-GlcNAcylation) is a dynamic, inducible post-translational modification (PTM) of thousands of intracellular proteins. There are only two enzymes responsible for O-GlcNAc cycling in higher eukaryotes, O-GlcNAc transferase (OGT) and O-GlcNAcase (OGA), which catalyze addition and removal, respectively. We hypothesized that constructing OGT substrate/interactor networks could serve as a useful foundation for understanding the functions of O-GlcNAcylation. Moreover, this approach might reveal novel insights into how OGT is able to coordinate the specific modification of thousands of proteins in response to individual stimuli.

Here, we first sought to validate interactor-substrate relationships suggested by these networks. Specifically, we found that knockdown (KD) of OGT interacting proteins was sufficient to disrupt O-GlcNAcylation of non-interacting OGT substrates. KD of the OGT interacting protein BAP1 changed the O-GlcNAcylation of several of its interactor proteins, many of which do not themselves interact with OGT. This KD strategy was attempted with other potential adaptor proteins such as WDR5 and CDK9, but KD was unsuccessful. KD of the OGT interacting protein GIT1 lead to intriguing changes in the O-GlcNAcylation of liprin-α1. Both of these proteins are vital for synaptic function in excitatory neurons. This result appears significant to the latter protein's function as it changes with neuronal activity. The aforementioned two findings suggest that association between OGT and its interactors may allow OGT to engage different sets of substrates in different contexts.

Further, we investigated whether modulating global O-GlcNAcylation can affect peroxisome and lipid droplet biogenesis and function, a potentially novel role for O-

GlcNAcylation revealed by our network. Together, these studies demonstrate that our networking approach highlights functional connections between OGT interactors and substrates.

Table of Contents and Figures

Chapter 1: Introduction

Numerous neurodegenerative and hepatic disorders have links to energy metabolism.[1,2] For instance, Alzheimer's disease (AD) is a neurodegenerative disorder that affects upwards of 5.7 million Americans, a number that is expected to double by 2050.[3] One noteworthy characteristic of the disorder is that reduced brain glucose metabolism precedes the onset of other symptoms.[4] Similarly, many hepatic disorders stem from impairments in peroxisome fatty acid metabolism and lipid droplet regulation, which feeds into glucose metabolic pathways.[5–7] In particular, type 2 diabetes mellitus (T2DM) is characterized by a dysregulation of glucose metabolism impacted by fatty acid metabolism in liver peroxisomes.[2,6,8] One potential consequence of altered glucose metabolism is altered O-linked β-*N*-acetylglucosamine glycosylation (O-GlcNAcylation). In fact, decreased O-GlcNAcylation has been observed in AD brains, suggesting that loss or reduction of O-GlcNAc may play a major role in AD pathogenesis.[4] Additionally, O-GlcNAcylation has been observed to change in response to glucose availability in the liver.[2,5,8–10] This, along with observed alterations in O-GlcNAcylation in mouse models of diabetes, have indicated that O-GlcNAcylation may play an important role in the disorder.[1]

O-GlcNAcylation is a dynamic, inducible post-translational modification of serine and threonine residues (Figure 1.1).[11,12] Unlike most sugars, O-GlcNAc is localized to the cytoplasm,

mitochondria, and nucleus, allowing it to affect and be affected by numerous intracellular processes.[11–13] O-GlcNAcylation is vital to development, as OGT knock out is embryonic lethal.[14] UDP-GlcNAc, the donor sugar for O-GlcNAcylation, lies at the end of the hexosamine biosynthetic pathway (HBP), which integrates carbohydrate, lipid, ketogenic amino acid, and nucleic acid metabolic pathways, indicating that the modification may play a role in sensing nutrient availability.[13,15,16] Due to all of the aforementioned properties, O-GlcNAc is uniquely suited to play a dynamic role a wide variety of processes such as transcriptional regulation, neuronal function, and nutrient sensing.[11] Clearly, a better understanding of how O-GlcNAcylation is regulated and the specific roles it plays would elucidate a significant component of cellular functioning.

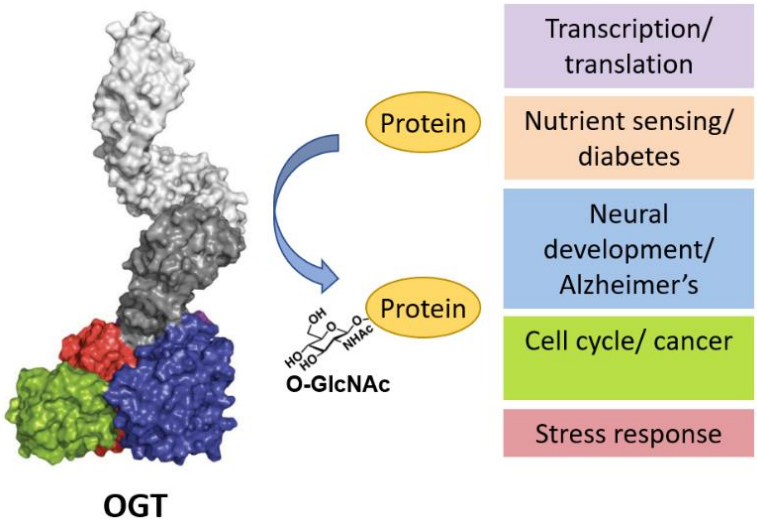

Figure 1.1: Significance of O-GlcNAcylation. OGT covalently modifies serine and threonine residues of proteins with O-GlcNAc. This modification impacts a variety of functions. Adapted from Lazarus et al. 2011 and Hart et al. 2011.

Interestingly, O-GlcNAcylation is finely regulated in response to stimuli, similar to phosphorylation.[11] However, unlike phosphorylation, which is regulated by diverse families of kinases and phosphatases, only a single pair of enzymes, O-GlcNAc transferase (OGT) and O-GlcNAcase (OGA), are responsible for O-GlcNAc cycling in higher eukaryotes.[4,12] Therefore, it remains an open question how just two enzymes can select among thousands of substrates to specifically regulate O-GlcNAcylation in response to stimuli. One proposed mechanism is that the dynamic interaction of OGT and OGA with adaptor proteins can 'target' these enzymes to certain

substrates, constraining under what conditions and at which sites O-GlcNAc cycling can occur (Figure 1.2).[17,18]

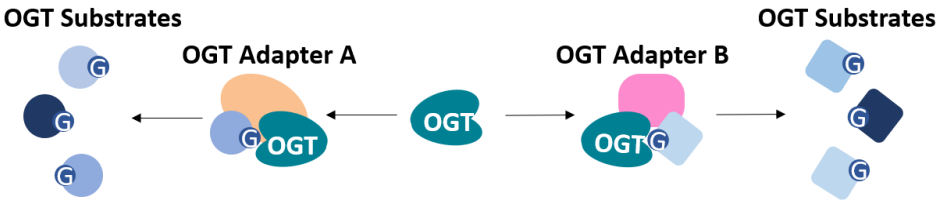

Figure 1.2: Adapter Protein Hypothesis. OGT interacts with different subsets of its substrates via different adapter proteins. This can confer the highly controlled specificity observed in protein O-GlcNAcylation.

To investigate the OGT adaptor protein hypothesis, our lab developed a technique to identify potential adaptor proteins (Figure 1.3).[19] O-GlcNAcylated proteins are chemically tagged with biotin via a chemoenzymatic labeling technique,[20] enriched via streptavidin capture, and identified via mass-spectrometry (MS) based O-GlcNAc proteomics. OGT interactors are identified via tandem affinity purification-MS. These two sets of proteins are then organized into a protein-protein interaction (PPI) network in CytoScape (using two PPI databases, BioGRID and IntAct) and partitioned into subgroups in an unsupervised manner using the community clustering algorithm GLay.[21,22] We hypothesized that we

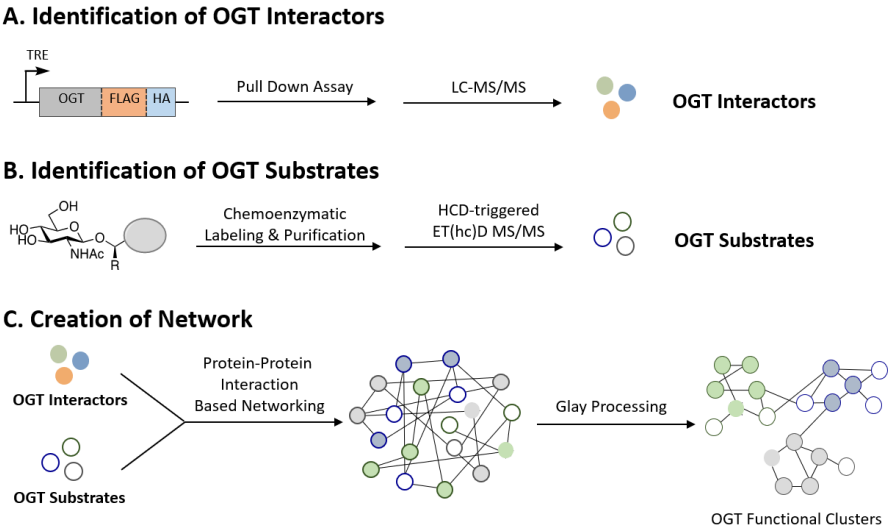

Figure 1.3: Creation of OGT Substrate/Interactor Networks. A Tissue from mice expressing FLAG and HA tagged OGT was used to conduct a pull down assay to capture any proteins associated with OGT, followed by LC-MS/MS to identify OGT interactors. **B** Chemoenzymatic labeling was used to tag O-GlcyNAcylated proteins from the same tissues as (A). These OGT substrate proteins were purified and identified by HCD-triggered ET(nc)D MS/MS. **C** Protein-protein interaction based networking was used to combine the interactor and substrate data, and Glay was used to identify OGT functional clusters.

could then identify potential OGT adaptor proteins by finding interactors that themselves interacted with many OGT substrates, especially those substrates which do not directly interact with OGT. This technique was carried out on whole brain lysates, liver lysates, and human embryonic kidney 293T (HEK 239T) cell lysates to yield three networks of OGT interactors and substrates.

Each of these networks yielded many results that we believed merited further study. For instance, the HEK 293T network contained three subnetworks related to transcriptional regulation that stood out as particularly interesting to investigate: that of BAP1, the PR-DUB complex, and its interactors (Figure 1.4A); WDR5 and its interactors including the SET1 complex (Figure 1.4B); and CDK9 and its interactors (Figure 1.4C). In each case, the former protein is an OGT interactor that itself interacts with many OGT substrates. Many of these substrates do not themselves directly interact with OGT. This O-GlcNAcylation pattern suggested that the former protein could function as an adaptor protein for the latter set of proteins. The polycomb repressive

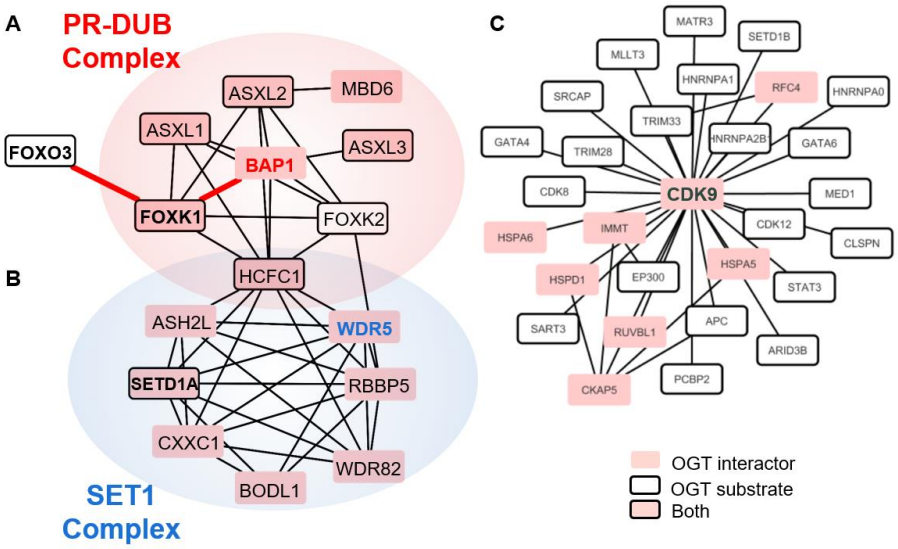

Figure 1.4: BAP1, WDR5, and CDK9 Subnetworks. The proteins in pink boxes interact with OGT. Boxes with thick borders indicate that the protein is O-GlcNAcylated. These data were taken from the 293T cell network, but the relationships are present in other tissue networks as well. **A BAP1 Subnetwork.** Note that ASXL1, FOXK1, FOXK2 (components of the PR-DUB complex), and FOXO3 are O-GlcNAcylated but do not all interact with OGT. **B WDR5 Subnetwork.** Note that FOXK2 is an OGT substrate but not an interactor. WDR5 Interacts in a number of other complexes (not shown) with similar O-GlcNAcylation patterns. **C CDK9 Subnetwork.** Note that MLLT3, SART3, and many other proteins are O-GlcNAcylated, do not interact with OGT, but do interact with CDK9.

deubiquitylase (PR-DUB) complex, particularly the deubiquitinase BRCA-associated protein 1 (BAP1), is responsible for histone H2A deubiquitinylation, which plays an important role in gene expression.[23] WD repeat-containing protein 5 (WDR5) has been suggested to serve as a scaffold protein for multiple complexes including the histone-lysine N-methyltransferase, H3 lysine-4 specific (SET1) complex and is known to play a role in histone H3 methylation.[24–26] Both of these subnetworks also appeared in the brain and liver networks, suggesting that O-GlcNAcylation of these proteins is important to gene regulation of all three tissue types. Cyclin-dependent kinase 9 (CDK9) is a member of two transcriptional elongation-regulating complexes: the Super Elongation Complex (SEC) and the 7SK snRNP inactive complex.[27–29] Investigations into these three subnetworks are discussed in Chapter 2.

The brain network contained multiple notable subgroups correlated with different neuronal functions. One particularly interesting subnetwork was enriched for postsynaptic density (PSD) proteins including ARF GTPase-activating protein GIT1 (GIT1) and the liprin-α (PPFIA) family of proteins. The PSD is a region of a neuron's dendrite that receives signals and plays a role in synaptic plasticity. The liprin-α family and GIT1 are known to play a role in maintaining the structure of the PSD.[30] The GIT1 subnetwork had an O-GlcNAcylation pattern suggesting a putative adaptor protein similar to that described above: GIT1 interacts with OGT and the OGT

substrates liprin-α1-4, which themselves (except liprin-α3) do not interact directly with OGT (Figure 1.5). Investigations into this system and its effect on liprin-α1 function are discussed in Chapter 3.

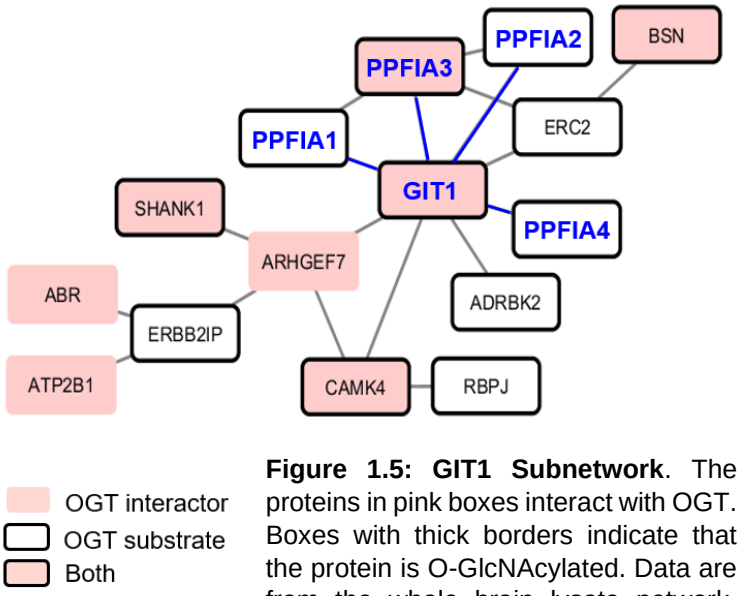

Figure 1.5: GIT1 Subnetwork. The proteins in pink boxes interact with OGT. Boxes with thick borders indicate that the protein is O-GlcNAcylated. Data are from the whole brain lysate network. Note that liprin-α 1, 2, and 4 (PPFIA1, 2, and 4) are O-GlcNAcylated but do not interact with OGT.

The liver network not only produced results similar to those above suggesting potential adaptor proteins but revealed new cellular functions for O-GlcNAcylation. One subnetwork

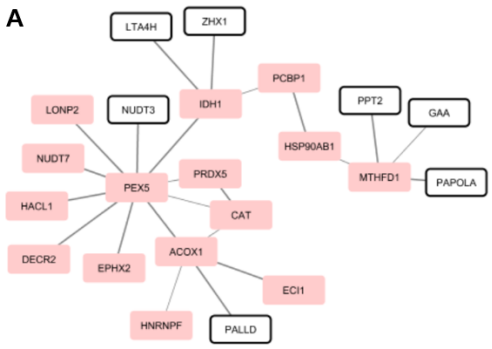

B

Site Rank	O-GlcNAcylation Fold Change
17	+4.5042
23	+4.02
28	+3.257
34	+3.0481
75	+2.122

Site Rank	O-GlcNAcylation Fold Change
89	+2.0115
94	+1.9586
104	+1.8549

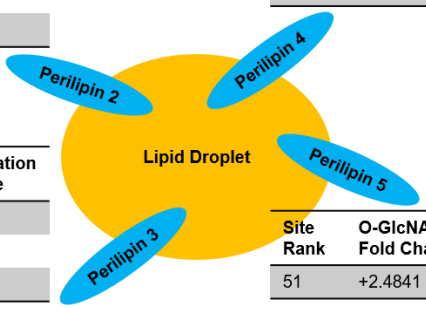

Site Rank	O-GlcNAcylation Fold Change
3	+14.033
4	+13.418
5	+11.072
6	+10.818
9	+ 8.3227

Site Rank	O-GlcNAcylation Fold Change
51	+2.4841

Figure 1.6: Peroxisome Subnetwork and Perilipin O-GlcNAcylation Changes. The proteins in pink boxes interact with OGT. Boxes with thick borders indicate that the protein is O-GlcNAcylated. Peroxisome data are from the hepatic tissue network and perilipin data are from changes in O-GlcNAcylation between normal and db/db mice..**A** The hepatic tissue network was enriched for several peroxisomal proteins including peroxisomal targeting signal 1 receptor (PEX5) and peroxisomal acyl-coenzyme A oxidase 1 (ACOX1). **B** The fold changes for O-GlcNAcylation sites of several proteins involved in fatty acid processing are shown. Notably, five of the top ten fold changes in O-GlcNAcylation were in the lipid metabolism-related protein perilipin 4. The perilipin family in particular all showed large fold changes in O-GlcNAcylation.

contained many proteins with roles in peroxisome organization and function (Figure 1.6.A) which had not been previously linked to O-GlcNAcylation.[19] Peroxisomes have multiple functions in cellular metabolism including portions of fatty acid metabolism and processing of reactive oxygen species.[31] Both of these processes are intimately linked to glucose metabolism, with the former feeding into it and the latter being a byproduct of the process. To further investigate phenomena related to the role of O-GlcNAc in liver function, O-GlcNAcylation levels of proteins in hepatic lysates from control and db/db mice (a mouse model of T2DM) were compared.[32] The perilipin family of proteins contained many of the top increased O-GlcNAcylation sites in the livers of db/db mice (Figure 1.6.B). The perilipins play a key role in fatty acid metabolism, as they are responsible for regulation of lipid droplet size and dynamics.[7,33–35] Lipid droplets store neutral fatty acids and are one of the main sites for their metabolism.[7,36] Both the peroxisome and lipid droplet data are consistent with O-GlcNAc's function as a nutrient sensor. Further investigations into these systems are discussed in Chapter 4.

Here, we aimed to validate the utility of our networking approach for identifying key proteins of interest in the study of O-GlcNAcylation. We did this by investigating examples of (1) potential adaptor proteins identified by our network, (2) the role an adaptor protein may play in the functioning of its interactors, and (3) the effect of O-GlcNAcylation on previously unstudied functions identified by our network. Together, these experiments not only demonstrate the utility of our networking approach for identifying adaptor proteins but reveal new information about the effects of O-GlcNAcylation on cellular functions.

Chapter 2: Validation of BAP1, WDR5, and CDK9 as Putative OGT Adaptor Proteins

2.1: Introduction

As discussed above, the mechanism by which OGT confers specificity in O-GlcNAcylation of its over one thousand substrates is an open problem. One promising hypothesis is that adaptor proteins allow OGT to associate with different subsets of its substrates and thereby create the observed specificities in both substrate choice and timing of O-GlcNAcylation in response to cellular conditions. To further our understanding of the relationships between the proteins involved, our lab created networks of OGT interactors and substrates.[19] These networks were created for multiple tissue types including HEK 293T cells, whole brain lysates, and liver lysates. Using these networks, we identified numerous potential adaptor proteins involved in transcriptional regulation for further investigation.

In all three networks, proteins in the Polycomb repressive deubiquitylase (PR-DUB) complex, particularly the deubiquitinase BRCA-associated protein 1 (BAP1), showed an interesting O-GlcNAcylation pattern (Figure 2.1.A).[19] That is, OGT has numerous substrates that it does not interact with, but BAP1 and/or the PR-DUB complex do interact with these substrates as well as OGT. This pattern suggests that the BAP1-OGT interaction may be necessary for the O-GlcNAcylation of other proteins in the complex. Thus, BAP1 may function as an adaptor protein for the O-GlcNAcylation of other members in the PR-DUB complex. The PR-DUB complex and its associated proteins play a key role in histone H2A deubiquitinylation, which impacts gene expression.[23] The interaction of this complex with OGT is also known to influence hepatic gluconeogenesis which may be involved T2DM pathogenesis.[12,24,37]

The protein WD repeat-containing protein 5 (WDR5) shows a similar O-GlcNAcylation pattern in that it is and OGT interactor that interacts with OGT substrates but is not itself an OGT substrate (Figure 2.1.B).[19] This

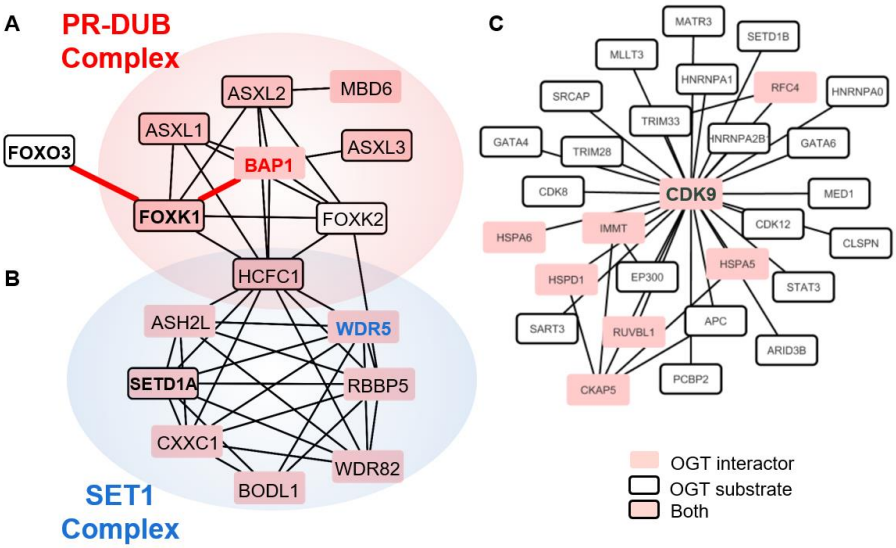

Figure 1.4: BAP1, WDR5, and CDK9 Subnetworks. The proteins in pink boxes interact with OGT. Boxes with thick borders indicate that the protein is O-GlcNAcylated. These data were taken from the 293T cell network, but the relationships are present in other tissue networks as well. **A BAP1 Subnetwork.** Note that ASXL1, FOXK1, FOXK2 (components of the PR-DUB complex), and FOXO3 are O-GlcNAcylated but do not all interact with OGT. **B WDR5 Subnetwork.** Note that FOXK2 is an OGT substrate but not an interactor. WDR5 Interacts in a number of other complexes (not shown) with similar O-GlcNAcylation patterns. **C CDK9 Subnetwork.** Note that MLLT3, SART3, and many other proteins are O-GlcNAcylated, do not interact with OGT, but do interact with CDK9.

suggests that WDR5 may function as an adaptor protein as well. WDR5 is also important for histone modification, though it plays a role in histone H3 methylation rather than H2A deubiquitinylation.[24,25] WDR5 is vital for the functioning of the complexes it plays a part in and has been suggested to be an important scaffold protein.[24,26] Additionally, OGT had already been identified as a subunit of WDR5 complexes, particularly the SET1 complex highlighted in Figure 2.1.B.[24] These data are consistent with our hypothesis that WDR5 could serve as an adaptor protein for many of its interactors that are also OGT substrates.

Similarly, the O-GlcNAcylation pattern of the protein CDK9 and its interactors in the HEK 293T cell network indicate that CDK9 might serve as an adaptor protein (Figure 2.1.C).[19] Like BAP1, many CDK9 interactors are OGT substrates, but not OGT interactors, suggesting that

CDK9 serves as an adaptor protein for their O-GlcNAcylation. In particular, the OGT substrates MLLT3 and SART3 were of particular interest due to their interactions with CDK9 to perform an important roles in transcriptional regulation.[29] CDK9 and MLLT3 are both members of the Super Elongation Complex (SEC), and CDK9 and SART3 are both members of the 7SK snRNP inactive complex, both of which regulate the transcriptional elongation stage of transcription.[27,28]

To determine whether BAP1, WDR5, and CDK9 might be adaptor proteins for O-GlcNAcylation of their interactors, we planned to knock down (KD) each one in 293T cells via transfection with siRNA, label O-GlcNAcylated proteins via chemoenzymatic labeling, and determine if there is a change in O-GlcNAcylation of the OGT substrates each is a potential adaptor protein for. By determining if there was a noteworthy change in O-GlcNAcylation of these proteins, this project served the twofold goal of validating the networks' ability to suggest interesting systems to study and identify putative OGT adaptor proteins.

2.2: Methods

Chemoenzymatic Labeling

We have previously developed and characterized a chemoenzymatic labeling process to attach various tags to the O-GlcNAc sugar modification.[20] This procedure uses an engineered bovine β-1,4-galactosyltransferase (Y289L GalT) to specifically and quantitatively append an unnatural azido sugar, N-azidoacetylgalactosamine (GalNAz), to O-GlcNAc residues. O-GlcNAcylated proteins labeled with GalNAz can then be further functionalized bioorthogonally via either the copper-catalyzed azide-alkyne cycloaddition (CuAAC) (Figure 2.2) or the strain-promoted azide-alkyne cycloaddition (SPAAC) reactions.[20] With both methods, there are multiple types of tags that can be used to functionalize the proteins, such as high-molecular-weight polyethylene glycol (PEG) 'mass tags' and biotin.[20] Here, the SPAAC method was used to elaborate O-GlcNAcylated proteins with the biotin tag for subsequent enrichment of labeled proteins via streptavidin capture. See Appendix A for more information.

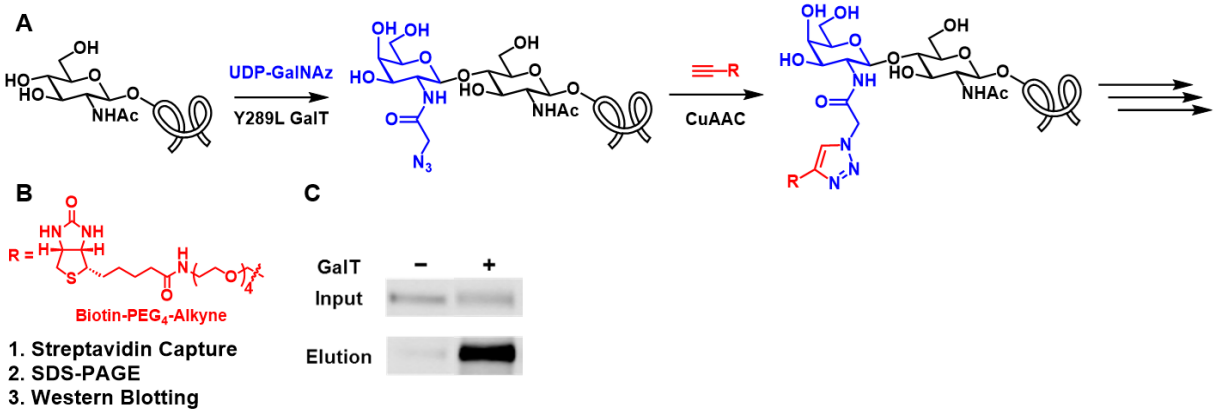

Figure 2.2: Chemoenzymatic labeling of O-GlcNAcylated proteins. A Incubation of O-GlcNAcylated proteins with Y289L GalT and uridine diphosphate N-azidoacetylgalactosamine (UDP-GalNAz) installs a chemical handle that can be further functionalized with alkyne-containing biotin probes using copper-catalyzed azide-alkyne cycloaddition (CuAAC, shown) or strain-promoted azide-alkyne cycloaddition (SPAAC, not shown). **B** Functionalization with biotin allows for selective enrichment and purification of O-GlcNAcylated proteins by streptavidin capture. **C** Sample Western Blot of CREB labeling. Adapted from Thompson et. al. 2017.

Transfection

HEK 293T cells were grown on a Poly-D-Lysine (PDL) coated plate and treated at 50% confluency with siRNA for the protein of interest or a scrambled sequence using MISSION siRNA transfection reagent and protocols to package the DNA for cellular uptake. Cells were incubated for 48 hours to allow sufficient time for gene silencing and protein degradation, after which their media was exchanged. The cells were lysed as described in Appendix A. The lysates were run on SDS-PAGE followed by Western Bloting for the protein of interest with α-tubulin as a control to evaluate KD efficiency.

2.3: Results

To determine if BAP1 serves as an adaptor protein, we transfected HEK 293T cells with siRNA to KD the protein. After optimization, we achieved 44-58% KD in two sets of cells and performed chemoenzymatic labeling on the lysates (Figure 2.3). In both cases, we did not observe significant changes in O-GlcNAcylation of PR-DUB complex proteins, but we did observe significant changes in FOXO3 O-GlcNAcylation. FOXO3 is a secondary interactor of BAP1 but a primary interactor of the PR-DUB complex, indicating that the complex itself might serve as an

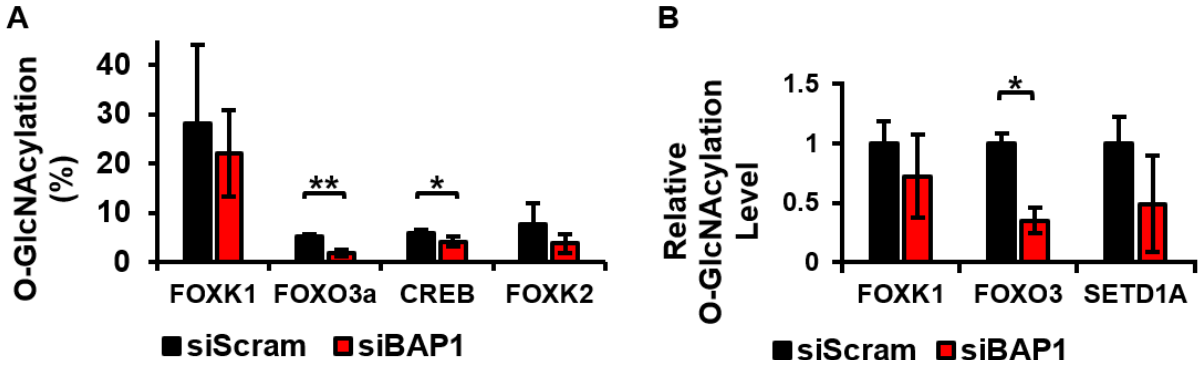

Figure 2.3: BAP1 KD O-GlcNAcylation. O-GlcNAcylation following two different BAP1 KD experiments are shown. **A** FOXO3a and CREB O-GlcNAcylation change significantly, while that of FOXK1 and FOXK2 do not. However, the variability in FOXK1 O-GlcNAcylation as well as the fact that the negative control of CREB had a significant change lead us to repeat the experiment. **B** FOXO3a O-GlcNAcylation had a statistically significant change, while that of FOXK1 and SETD1A did not. The high variability suggested that these data were insufficient to make concrete conclusions.

adaptor protein (Figure 2.4). However, the high variability in O-GlcNAcylation of some proteins as well as the significant change in CREB O-GlcNAcylation, which we did not expect to be affected, indicated that further experiments were needed to confirm these results.

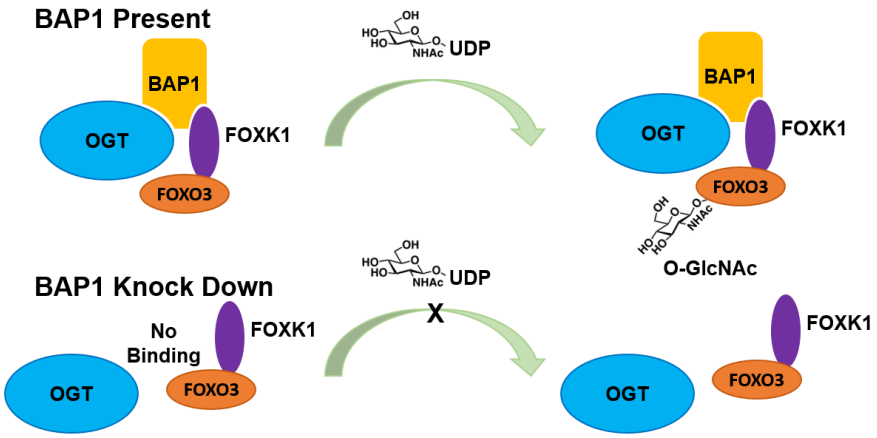

Figure 2.4: BAP1 Knock Down Hypothesis. We hypothesize that the PR-DUB complex acts as an adapter for OGT to O-GlcNAcylate FOXO3. Thus, we expect BAP1 KD to reduce FOXO3 O-GlcNAcylation.

Efforts to achieve WDR5 and CDK9 KD using the same method and conditions as the BAP1 KD were unsuccessful. Further, generation of a CDK9 KO line using the same method as the BAP1 KO line was unsuccessful. Thus, we were unable to test our hypotheses regarding WDR5 and CDK9 as adaptor proteins for their interactors.

2.4 Conclusion and Future Directions

We successfully knocked down BAP1 and found that BAP1 KD significantly decreased FOXO3 O-GlcNAcylation, indicating that this system was of interest for further study despite variable results. The WDR5 and CDK9 KDs were unsuccessful. The difficulty in creating KD or KO of these proteins may be due to their vital roles in the cell leading to decreased viability after KD, though it should be noted that successful CKD9 KD has been achieved by other labs.[38] Future directions for this project involve examining O-GlcNAcylation changes of a BAP1 KO cell line, which would mitigate the potentially confounding variable of incomplete KD, and creating

comparable CDK9 and WDR5 KO cell lines for similar experiments. The experiments presented here served as a proof of concept that BAP1 KD lead to alterations in O-GlcNAcylation.

Chapter 3: Examination of Liprin-α1 O-GlcNAcylation, its Regulation by GIT1, and its Role in GRIP1 Binding.

3.1 Introduction

As discussed in Chapter 1, how OGT confers specificity in O-GlcNAcylation of its over one thousand substrates is an open problem. One promising hypothesis is that adaptor proteins allow OGT to associate with different subsets of its substrates, which would provide the observed specificities in both substrate choice and cellular conditions under which the modification occurs. To further our understanding of the relationships between the proteins involved, our lab created networks of OGT interactors and substrates.[19] Here, we wished to investigate an adaptor protein system in more depth and determine the effect this O-GlcNAcylation has on the function of a specific OGT substrate. In the brain network, there is a subgroup particularly enriched for proteins in the PSD. The PSD is the region of a neuron's dendrite that receives neuronal signals and is a key player in synaptic plasticity. A subnetwork including ARF GTPase-activating protein GIT1 (GIT1) and the liprin-α family of proteins is of particular interest because of their O-GlcNAcylation pattern (Figure 3.1).[19] The liprin-α proteins are all O-GlcNAcylated, but only liprin-α3 and GIT1 interact with OGT, suggesting that GIT1 may function as an adaptor

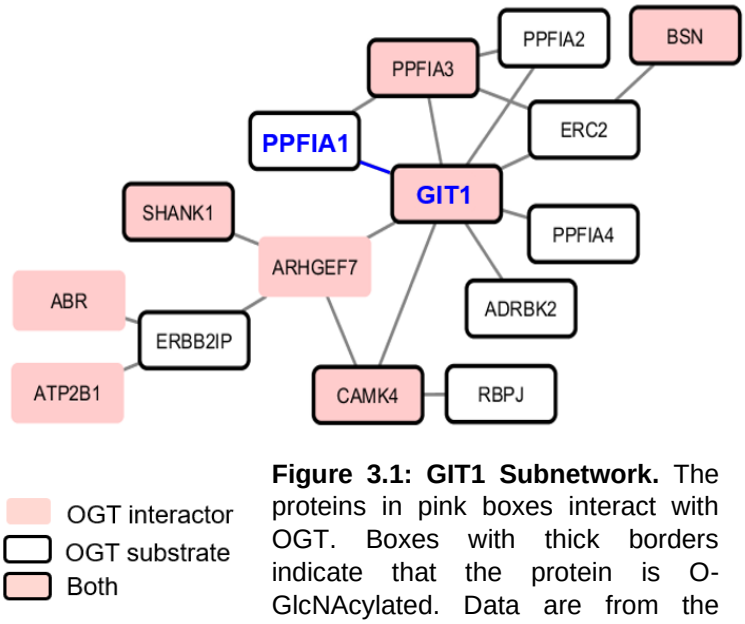

Figure 3.1: GIT1 Subnetwork. The proteins in pink boxes interact with OGT. Boxes with thick borders indicate that the protein is O-GlcNAcylated. Data are from the whole brain lysate network. Note that liprin-α 1, 2, and 4 (PPFIA1, 2, and 4) are O-GlcNAcylated but do not interact with OGT.

protein for the liprin-α family of proteins and is therefore necessary for their O-GlcNAcylation by OGT.

The liprin-α family and GIT1 are also important for maintaining the structure of the PSD.[30] In particular, liprin-α1 is involved in targeting α-amino-3-hydroxy-5-methyl-4-isoxazolepropionic acid receptors (AMPARs) to the synaptic membrane.[30,39] These glutamate-responsive ion channels are responsible for the majority of excitatory neurotransmission in the brain and are key players in the process of long-term potentiation (LTP), a primary mechanism for synaptic plasticity, learning, and memory.[30,40] To target AMPARs to the post-synaptic membrane, liprin-α1 must bind to glutamate receptor-interacting protein 1 (GRIP1), which binds to AMPARs (particularly the GluR2 subunit).[39–41] Interestingly, the only known O-GlcNAcylation site on liprin-α1 lies within the region known to mediate binding to GRIP1.[41] Furthermore, the crystal structure of liprin-α1 bound to GRIP1[41] suggests that O-GlcNAcylation of this site might prevent binding due to its steric bulk. Thus, we hypothesize that the O-GlcNAcylation of liprin-α1 might interrupt the binding between liprin-α1 and GRIP1. If true, this would indicate that when O-GlcNAcylation is decreased, levels of the liprin-α1 GRIP1 complex increase and result in more AMPARs being targeted to the synapse (Figure 3.2). Taken together, the aforementioned data suggest a potential role for liprin-α1 O-GlcNAcylation in LTP and synaptic organization. Here, we determined the dynamics of liprin-α1 O-GlcNAcylation in neurons, investigated the role of GIT1 as an adaptor protein in regulating liprin-α1 O-GlcNAcylation with neuronal stimulation, and began to examine

the effect of liprin-α1 O-GlcNAcylation on its binding with GRIP1.

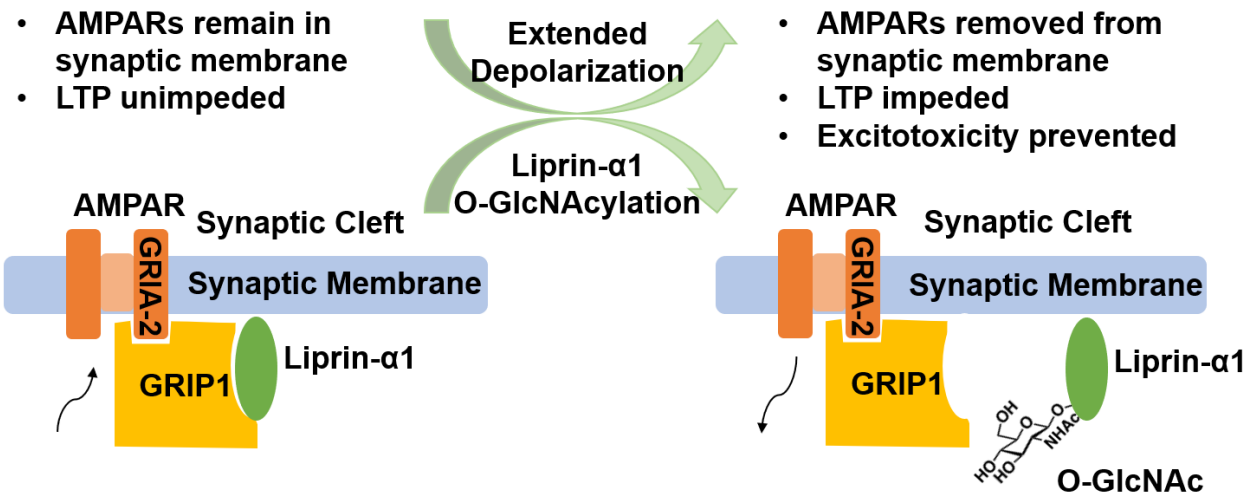

Figure 3.2: Overall Liprin-α1 O-GlcNAcylation Hypothesis. When liprin-α1 is not O-GlcNAcylated, we expect it to bind to GRIP1, which in turn continues targeting AMPARs to the synapse (left). We expect liprin-α1 O-GlcNAcylation, to inhibit its binding with GRIP1, which would reduce the number of AMPARs

3.2: Methods

Chemoenzymatic Labeling

We have previously developed and characterized a chemoenzymatic labeling process to attach various tags to the O-GlcNAc sugar modification.[20] This procedure uses an engineered bovine β-1,4-galactosyltransferase (Y289L GalT) to specifically and quantitatively append an unnatural azido sugar, N-azidoacetylgalactosamine (GalNAz), to O-GlcNAc residues. O-GlcNAcylated proteins labeled with GalNAz can then be further functionalized bioorthogonally via either the copper-catalyzed azide-alkyne cycloaddition (CuAAC) (Figure 2.2) or the strain-promoted azide-alkyne cycloaddition (SPAAC) reactions.[20] Here, the SPAAC method was used to elaborate the biotin tag for subsequent enrichment of labeled proteins via streptavidin capture. Quantities of protein used for the labeling experiments in Section 3.4 were decreased, so reaction and reagent volumes were decreased to compensate and maintain equivalent concentrations. See Appendix A for more details.

Co-Immunoprecipitation

Neurons expressing OGT-FH containing HA and FLAG tags were grown and either silenced or KCl stimulated. Cells were lysed after 26 days and diluted as preparation for the co-immunoprecipitation assay. Input lysate was saved for Western Blotting. The lysate was incubated with anti-FLAG magnetic beads, and protein was eluted. Inputs and eluents were run on SDS-PAGE and Western blotted for HA (one of the tags on OGT), liprin-α1 and GIT1. Pulldown efficiency was calculated by measuring the intensity of the eluent bands relative to the input. See Appendix A for more details.

Lentivirus Production

HEK 293T cells were transfected with GIT1 or scrambled shRNA-containing lentiviral plasmids, as well as lentiviral packaging plasmids, using Lipofectamine 3000 to package the DNA at 50-90% confluence according to manufacturer's instructions. The virus was harvested by collecting and replacing the media 24 and 48 hours post-transfection and concentrated using PEG precipitation.[42] The knockdown (KD) efficiency of the virus was validated by infecting primary mouse cortical neurons followed by lysis, SDS-PAGE, and Western blotting for GIT1. See Appendix A for more details.

3.3 Liprin-α1 O-GlcNAcylation Increases with Neuronal Depolarization

The data for the brain network was collected from whole brain lysates, so we first needed to confirm that liprin-α1 was O-GlcNAcylated in neurons specifically. To do this, we cultured mouse primary cortical neurons to maturity (21 DIV), then either silenced or stimulated them. This allowed us to determine if O-GlcNAcylation levels change with neural activity. We harvested the lysates and labeled O-GlcNAcylated proteins as described in Appendix A. Using this

methodology, we have shown that liprin-α1 is O-GlcNAcylated in neurons, and this O-GlcNAcylation increases with neuronal stimulation (Figure 3.3). This signifies that liprin-α1 O-GlcNAcylation may participate in regulating its role in neuronal function.

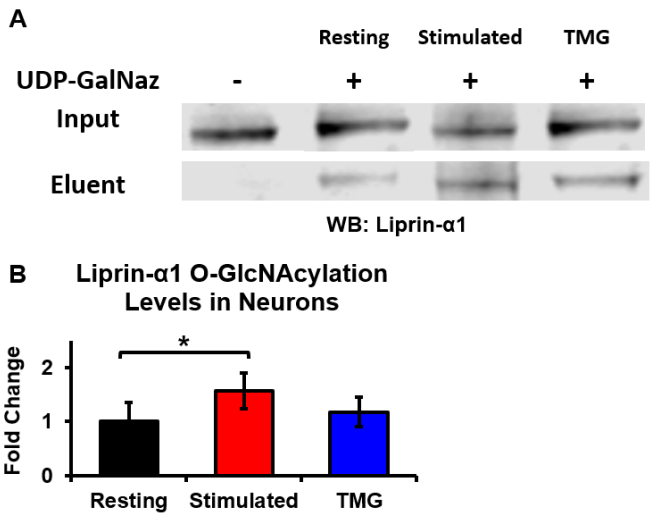

Figure 3.3: Liprin-α1 O-GlcNAcylation. Liprin-α1 O-GlcNAcylation in mouse primary cortical neurons. **A** Representative Western Blot of streptavidin capture enrichment of O-GlcNAcylated liprin-α1. **B** There was a significant increase in liprin-α1 O-GlcNAcylation with KCl stimulation, but not with TMG inhibition of OGA.
* $p < 0.05$; $n = 6$

3.4 Investigation of GIT1 as an Adaptor Protein

The previously discussed network of O-GlcNAcylated proteins in whole brain lysates indicated that GIT1, but not liprin-α1, is an interactor of OGT. To verify that this was true in mouse cortical neurons, neurons expressing FLAG- and HA-tagged OGT (OGT-FH) were either silenced or stimulated with KCl and lysed, before purifying OGT by immunoprecipitation. We then performed a Western blot on the samples from this experiment and confirmed that GIT1 does in fact co-IP with OGT, but liprin-α1 does not (Figure 3.4.A). There was no qualitative difference in OGT, GIT1, or liprin- α1 pull down between the silenced and stimulated conditions; a quantitative comparison was not possible due to the absence of an input sample for the silenced condition, so we replicated this experiment with an input sample present, which quantitatively yielded the same results (Figure 3.4.B). A nonspecific HA band from the OGT blot overlapped with the GIT1 signal,

so this set of data cannot be used to compare GIT1 stoichiometry. To the extent that can be shown by each of these experiments, KCl stimulation does not appear to change GIT1 association with OGT, indicating that the increase in liprin-α1 O-GlcNAcylation

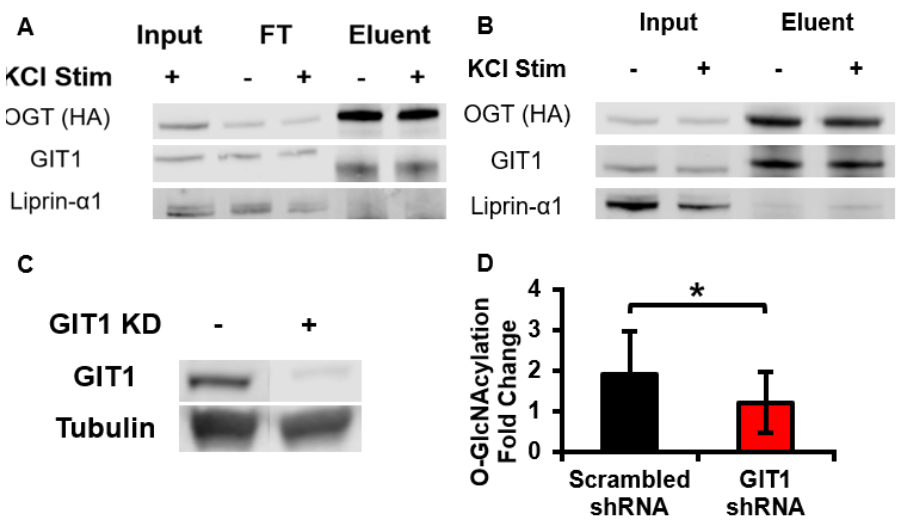

Figure 3.4: GIT1 KD and Liprin-α1 O-GlcNAcylation. A & B Verification of GIT1 as an OGT Interactor qualitatively **(A)** and quantitatively **(B)**. Co-IP was conducted on OGT labeled with HA from cells that were either silenced (-) or stimulated (+). GIT1 co-IPed with OGT, but liprin- α1 did not. **C** Representative Western Blot of GIT1 KD following treatment with GIT1 shRNA lentivirus. KD consistently reached 55-89% efficiency. **D** GIT1 KD prevents depolarization-mediated increase in liprin-α1 O-GlcNAcylation.
* $p < 0.05$; $n = 8$

previously observed during KCl stimulation was not necessarily due to greater association of GIT1 and OGT. These results indicate that GIT1 is a relatively stable interactor of OGT, while liprin-α1 only associates transiently, confirm the previously observed interaction between OGT and GIT1 using TAP-MS, and demonstrate for the first time that a significant portion of neuronal GIT1 is stably associated with OGT.

As previously mentioned, GIT1 is a potential OGT-adaptor protein and thus its presence may be necessary for liprin-α1 O-GlcNAcylation, including dynamic O-GlcNAcylation. In previous labeling experiments, liprin-α1 O-GlcNAcylaion increased with KCl stimulation, which mimics excitatory stimulation; if GIT1 is necessary for this process we would expect GIT1 KD to prevent this increase. To determine if GIT1 is required for liprin-α1 O-GlcNAcylation, we employed our previously validated lentiviral-mediated strategy to KD GIT1 in primary mouse

cortical neurons and assay liprin-α1 O-GlcNAcylation using chemoenzymatic labeling. Briefly, we have developed a lentivirus to deliver a short-hairpin RNA (shRNA) targeting GIT1 mRNA for degradation (Figure 3.4.C). We used the aforementioned chemoenzymatic labeling technique to attach a biotin tag and enrich O-GlcNAcylated proteins. Initial experiments have proven promising and indicated that GIT1 may regulate KCl stimulation-mediated liprin-α1 O-GlcNAcylation (Figure 3.4.D). Interestingly, while baseline liprin-α1 O-GlcNAcylation did not decrease significantly following GIT1 KD as expected, we observed that *dynamic* liprin-α1 O-GlcNAcylation did not occur with GIT1 KD. This indicates that GIT1 may mediate dynamic liprin-α1 O-GlcNAcylation (Figure 3.5). Overall, these data give evidence in support of the hypothesis that GIT1 acts as an adaptor protein for liprin-α1 O-GlcNAcylation, though more replicates would be necessary to be certain of the details.

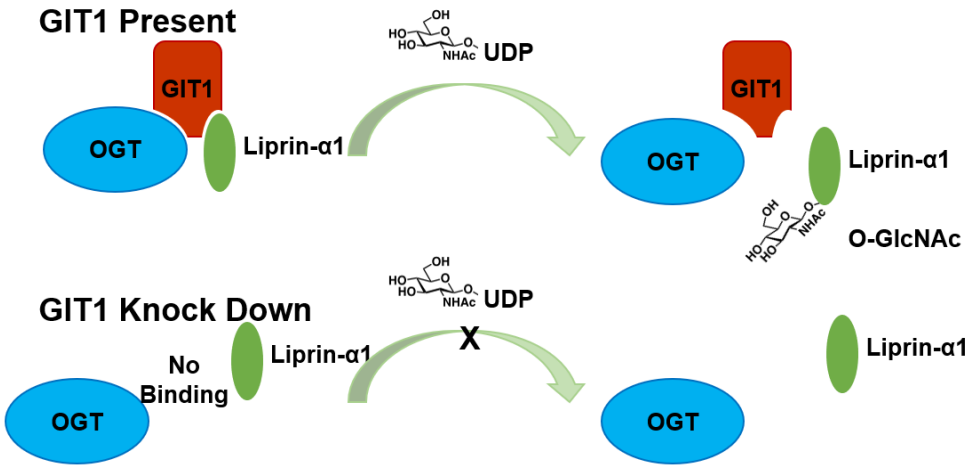

Figure 3.5: GIT1 KD Model. When GIT1 is present (top), OGT can interact with liprin-α1 to O-GlcNAcylate it when neurons are stimulated. When GIT1 is knocked down (bottom), this interaction cannot occur and liprin-α1 O-GlcNAcylation does not increase.

3.5 Determination of the Effect of Liprin-α1 O-GlcNAcylation on its Binding with GRIP1

Finally, to determine if liprin-α1 O-GlcNAcylation affects liprin-α1 binding with GRIP1, we planned to transfect cells to express mutant forms of liprin-α1 and exogenous GRIP1 and attempt to co-immunoprecipitate (co-IP) the two proteins. In the first experimental group, the O-GlcNAcylation site on liprin-α1 (T1263) will be replaced with a bulky amino acid (tryptophan) to mimic O-GlcNAcylation. If our hypothesis is correct, then we expect this mutant will have decreased binding to GRIP1. In the second experimental group, the liprin-α1 O-GlcNAcylation site will be replaced with the non-bulky amino acid, alanine, (that cannot be O-GlcNAcylated) to prevent O-GlcNAcylation. Here, we expect liprin-α1 to bind to GRIP1 more strongly than wild type (WT) liprin-α1. If successful, these experiments would strongly suggest that O-GlcNAcylation of liprin-α1 may actively regulate its binding to GRIP1 (Figure 3.6). Thus far, we

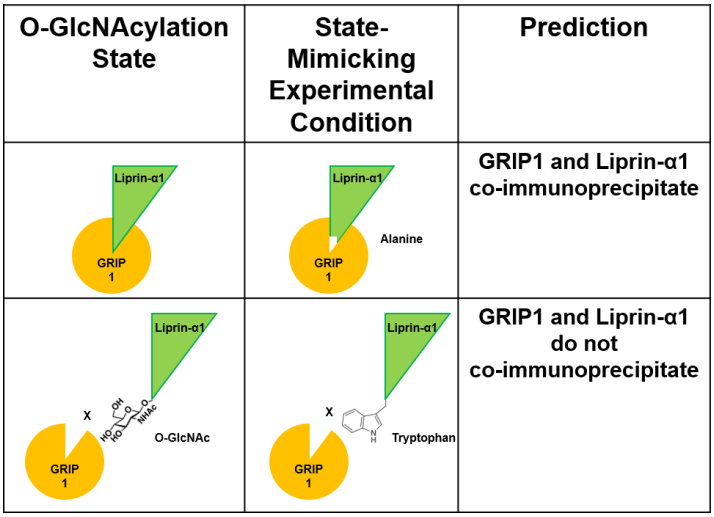

Figure 3.6: GRIP1 co-IP experimental design. By mimicking the naturally occurring O-GlcNAcylation states of liprin-α1 with single-residue mutants, we will demonstrate whether the O-GlcNAc modification affects GRIP1 binding.

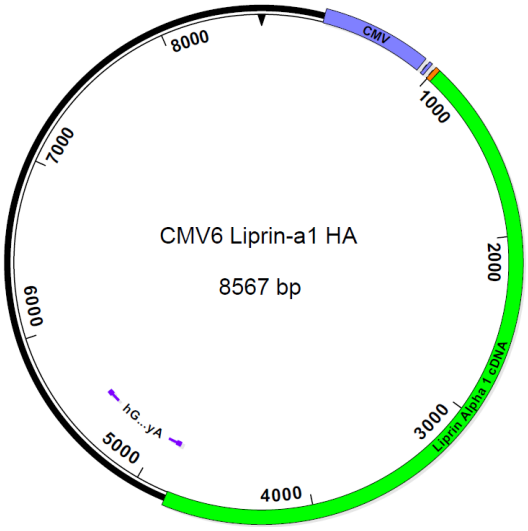

Figure 3.7: Plasmid map of Liprin-α1 expression vector. Liprin-α1 (green) with an HA tag (orange) is contained within a CMV6 plasmid for expression in HEK 293T cells.

created a construct containing WT liprin-α1 (Figure 3.7), have designed the mutagenesis to create the single amino acid replacement liprin-α1 constructs, and designed the GRIP1 construct. Future experiments would use the above outlined methods to create the remaining constructs, transfect HEK 293T cells with them, and run the co-IP.

3.6 Conclusion and Future Directions

Liprin-α1 is O-GlcNAcylated in neurons, and this O-GlcNAcylation increases with neuronal stimulation. This signifies that liprin-α1 O-GlcNAcylation may participate in regulating its role in neuronal function. GIT1 may also mediate dynamic liprin-α1 O-GlcNAcylation. In the future, these experiments should be repeated in order to have higher confidence in our results. Additionally, the creation and testing of the liprin-α1 and GRIP1 constructs will need to be finished, and the co-IP experiment conducted. Overall, these experiments not only demonstrated the utility of our networking approach for identifying a potential adaptor protein but revealed new information about the properties of liprin-α1 O-GlcNAcylation.

Chapter 4: Effects of Global Modulation of O-GlcNAcylation on Fat Metabolism, Peroxisome Structure, and Lipid Droplet Structure.

4.1: Introduction

As discussed in Chapter 1, numerous lines of evidence have suggested that O-GlcNAc functions as a nutrient sensor.[43] To further our understanding of O-GlcNAcylation, our lab created networks of OGT interactors and substrates for multiple tissue types including liver lysates.[19] This liver network uncovered new cellular functions for O-GlcNAcylation related to its nutrient sensor role. In particular, it contains a cluster enriched for proteins involved in peroxisome organization and function (Figure 4.1.A), which have not been previously tied to O-GlcNAcylation.[19] Peroxisomes are responsible for portions of fatty acid metabolism that feed into glucose metabolism and processing of reactive oxygen species (a byproduct of glucose metabolism).[31] Additionally, there are several clusters in the liver network enriched for proteins involved in fatty acid metabolism, especially very-long- and long-chain fatty acid metabolism that takes place in peroxisomes, indicating that O-GlcNAcylation may play a role in the process as well.

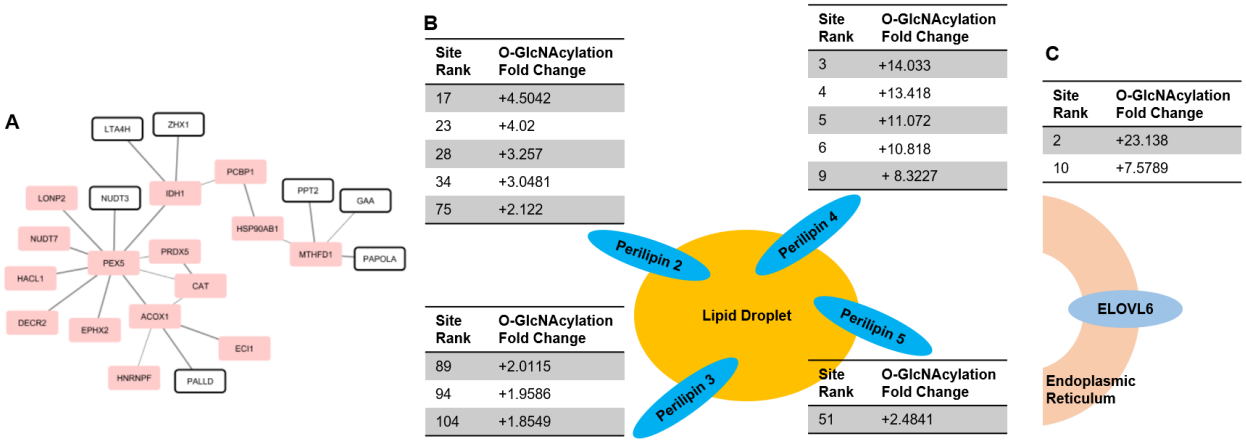

Figure 4.1: Peroxisome Subnetwork and Perilipin O-GlcNAcylation Changes. The proteins in pink boxes interact with OGT. Boxes with thick borders indicate that the protein is O-GlcNAcylated. Peroxisome data are from the hepatic tissue network and perilipin data are from changes in O-GlcNAcylation between normal and db/db mice..**A** The hepatic tissue network was enriched for several peroxisomal proteins including peroxisomal targeting signal 1 receptor (PEX5) and peroxisomal acyl-coenzyme A oxidase 1 (ACOX1). **B & C** The fold changes for O-GlcNAcylation sites of several proteins

To further investigate the role of O-GlcNAc in liver function, O-GlcNAcylation levels of proteins in hepatic lysates from control and db/db mice (a mouse model of T2DM) were compared.[32] Briefly, chemoenzymatic labeling (described in Chapter 2) was used to tag and purify O-GlcNAcylated proteins from the two types of lysates. Mass spectrometry was used to identify labeled proteins and quantify O-GlcNAcylation at each site. Ratios of these O-GlcNAcylation levels between the two conditions for each site were calculated.

This screen demonstrated that the O-GlcNAcylation of several perilipin family proteins was significantly increased in the livers of db/db mice (Figure 4.1.B).[32] Lipid droplets are critical sites for neutral fatty acid storage and metabolism.[7,36] Perilipins help regulate lipid droplet size and dynamics, which is vital for proper fatty acid metabolism.[7,33–35] Previous studies have suggested that O-GlcNAcylation of members of the perilipin family of proteins is involved in regulation of lipolysis in visceral fat tissue,[34] though perilipin O-GlcNAcylation had not yet been examined in liver tissue. Perilipin 2, which possesses five of the increasing O-GlcNAcylation sites, is known to be at least in part regulated by peroxisome proliferator-activated receptor α (PPARα) and γ in liver tissues.[36,44] This raises the possibility that the O-GlcNAcylation of proteins involved in peroxisome and lipid droplet formation and function might regulate fatty acid biosynthesis and storage. Perilipin 4, which possesses five of the top ten changing O-GlcNAcylation sites in our screen, is known to be involved in lipid droplet formation, though the exact functions of this protein have not yet been determined.[36] Though not a perilipin itself, one of the other proteins in the db/db mice O-GlcNAcylation fold change screen containing the two of the top ten sites was elongation of very long chain fatty acids protein 6 (Elovl6) (Figure 4.1.C).[32] This protein catalyzes the rate limiting step of long- and very long-chain fatty acid elongation.[45] While not directly related to perilipin function, this process is also very important to fat metabolism and has been implicated in

hepatic insulin sensitivity, though the exact effect it has and its regulation are unclear.[46] Further, altering O-GlcNAcylation can influence insulin signaling, glucose uptake, gluconeogenesis, and fatty acid metabolism, indicating that it has a vital role in these processes.[1,2,8,16,47]

Though the effects of O-GlcNAcylation on a few individual proteins involved in these processes are known, how this modification accomplishes these results and the overall role it plays in coordinating each of these processes as a whole has yet to be elucidated. Moreover, virtually nothing is known about the role of O-GlcNAc in peroxisome function despite it being intimately linked to many aspects of metabolism.[1,2,8,48] This, along with the aforementioned evidence that O-GlcNAc serves as a nutrient sensor and the liver network is particularly enriched in peroxisome and fatty acid metabolism proteins, suggests that O-GlcNAcylation may play a role in regulating peroxisome function. To investigate these phenomena, we used established methods to globally increase O-GlcNAcylation and subsequently sought to examine changes in long-chain fatty acid metabolism and determine differences in peroxisome and lipid droplet morphology.

4.2 In-vitro Assay for Fatty Acids

To determine the effect of O-GlcNAcylation on peroxisomes and/or fatty acid metabolism in hepatic cells, we grew human hepatocellular carcinoma (HepG2) cells in normal and hyperglycemic conditions. Cells from both conditions were treated with thiamet G (TMG),[49] a potent OGA inhibitor,

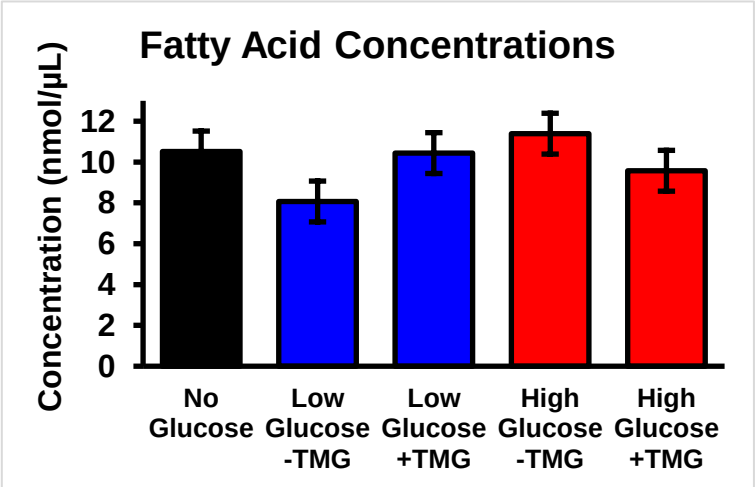

Figure 4.2: Fatty Acid Concentrations. Fatty acid concentrations of HepG2 lysates were measured using a long-chain fatty acid detection assay. No significant differences were observed between conditions.

to prevent O-GlcNAc cycling. To investigate effects on fatty acid metabolism, cell lysates were tested for long-chain and very-long-chain fatty acids after treatment and compared to an untreated control. Even after optimization to decrease variability, no significant differences between the conditions were observed (Figure 4.2). It is likely that any differences are too small for detection by the resolution of this test or that the cell is able to compensate for global O-GlcNAc modulation with respect to its fatty acid levels in the short term.

4.3 Characterization of Peroxisome and Lipid Droplet Morphology

Similarly treated cells as in section 4.2 were grown on cover slips for microscopy as described in Appendix A. These cells were fixed; stained with antibodies for PMP70, ACOX1, or catalase; and imaged by confocal microscopy. The PMP70 antibody did not noticeably stain any cellular component, and the ACOX1 antibody was not very specific and signal was present throughout the cytoplasm. However, the catalase antibody clearly stained peroxisomes. The images were promising, with peroxisomes clearly distinguishable (Figure 4.3).

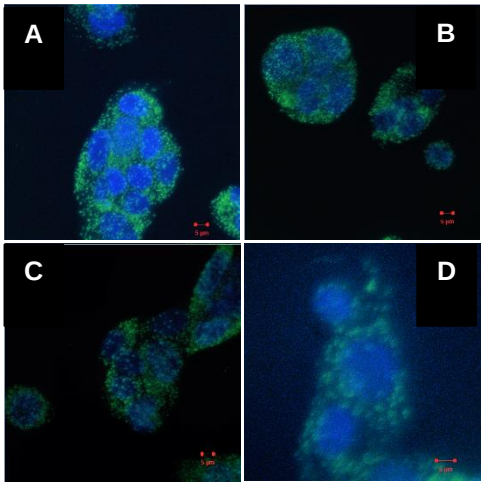

Figure 4.3: Representative Images of Peroxisome Imaging in HepG2 Cells. Maximum intensity projection images shown for all conditions. Nuclei were stained with 4′,6-diamidino-2-phenylindole (DAPI) and appear blue in these images. Peroxisomes were visualized with ACOX1 antibody and appear green in these images. **A** Low glucose condition imaged with 63x objective. **B** Low glucose and TMG treatment condition, imaged with 63x objective. **C** High glucose condition imaged with 63x objective. **D** High glucose and TMG treatment condition, imaged with 100x objective.

In order to examine lipid droplets at the same time as peroxisomes, another set of cells were stained for catalase and with 4,4-Difluoro-1,3,5,7,8-Pentamethyl-4-Bora-3a,4a-Diaza-s-Indacene (BODIPY). Peroxisomes were unable to be detected by microscopy, most likely due to a problem with the microscope laser that detected the secondary antibody used against the

catalase antibody. However, lipid droplet images were successfully obtained (Figure 4.4). Image processing was performed on these preliminary images to determine the success of this procedure and to create a data processing pipeline for larger scale tiled images. Image processing code was written to segment the images and identify lipid droplets (Appendix C), and the area of each droplet were determined (Figure 4.5). While there were slight differences between conditions, the standard deviations were too large to support any conclusions. However, the sample size was relatively small with only 10-15 cells per image, so a tiled image of the entire slide might be able to decrease this variance.

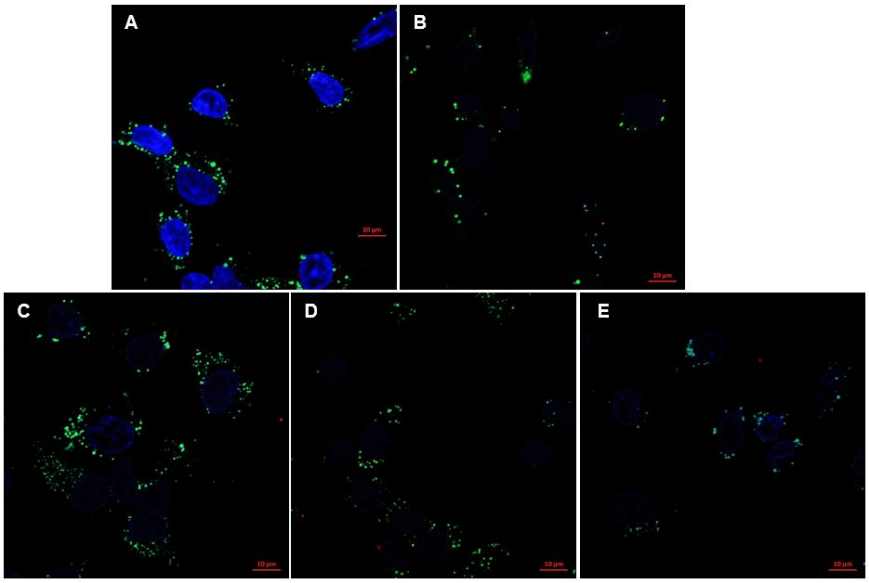

Figure 4.4: Representative Images of Lipid Droplet Imaging in HepG2 Cells. Nuclei were stained with 4′,6-diamidino-2-phenylindole (DAPI) and appear blue in these images. Lipid droplets were visualized with 4,4-Difluoro-1,3,5,7,8-Pentamethyl-4-Bora-3a,4a-Diaza-s-Indacene (BODIPY) and appear green in these images. All images were taken with 63x objective. **A** High glucose condition **B** High glucose and TMG treatment condition. **C** Low glucose condition. **D** Low glucose and TMG treatment condition. **E** No glucose condition.

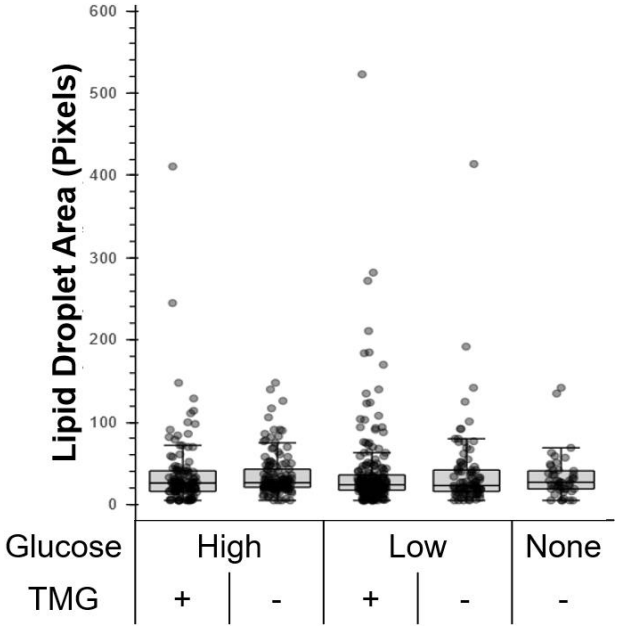

Figure 4.5: Representative Boxplot of Lipid Droplet Areas in HepG2 Cells. Areas of lipid droplets identified during image segmentation were measured for each of the conditions in three sets of images. Here, a representative set of data are shown. Notably, while the mean lipid droplet area differs between conditions, the variations are too large to support any conclusions.

4.4 Conclusion and Future Directions

The liver network and db/db liver screen both suggested novel roles for O-GlcNAc in fatty acid metabolism related to peroxisomes and lipid droplets, respectively. Bulk measurement of long- and very-long-chain fatty acids did not have fine enough resolution to detect differences due to global O-GlcNAc modulation, suggesting that such differences are either small or negated by feedback mechanisms on the timescale examined. Though we were unable to obtain significant data regarding the effect of O-GlcNAcylation on peroxisome morphology and lipid droplet size and number, we developed a method to investigate our hypothesis and process data from these experiments. Future investigations can implement these methods to create larger data sets that would likely decrease the variance observed.

Appendix A: Materials and Methods

Cell culture

Primary mouse cortical neurons were prepared as previously described,[50] plated on poly-d-lysine (PDL) coated plates, and cultured in Neurobasal medium (ThermoFisher) with 1% penicillin-streptomycin (P/S, ThermoFisher), 2mM GlutaMAX Supplement (ThermoFisher), and B-27 Plus (ThermoFisher). Half of the media was changed every 2-4 days. After 20 DIV, neuronal activity was silenced using tetrodotoxin (TTX, 10 μM, Tocris Biosciences) and D-AP5 (100 μM, Tocris Biosciences), treated with Thiamet-G (TMG, 50 μM, Sigma Aldrich), or treated with both TMG (50 μM) and glucosamine (50 mM, Sigma Aldrich). The following day, silenced neurons and those treated with both TMG and glucosamine were depolarized with KCl (60 mM) for 2 hours and subsequently lysed with either RIPA buffer or 2% SDS in HEPES pH 7.9, containing Roche c0mplete protease inhibitor cocktail (Sigma Aldrich), TMG (0.1 mM), and benzoase nuclease (Santa Cruz Biotechnology). The TMG treated neurons were lysed as described without treatment with KCl. In all cases, the protein concentration was measured using BCA assay (ThermoFisher).

HEK 293T cells were maintained in DMEM medium (Invitrogen) with 2 mM GlutaMAX, 100 U/mL penicillin-streptomycin (ThermoFisher), and 10% FBS (Invitrogen). Cells grown for transfection experiments were grown on poly-d-lysine (PDL) coated plates.

Hep G2 cells were plated on collagen-coated plates and maintained in DMEM medium (Invitrogen) with low glucose (1 mg/mL), 2 mM GlutaMAX, 100 U/mL penicillin-streptomycin (ThermoFisher), 10% FBS (Invitrogen), and without phenol red. Cells grown for microscopy were grown on cover slips coated with poly-d-lysine (PDL) followed by collagen-coating as described above.

Cell Staining

Hep G2 cells were grown as described above. At 50% confluency, cells were fixed using paraformaldehyde. Each well was stained with one of the following antibodies and the appropriate secondary antibodies: PMP70 (ThermoFisher, MA5-31368, 1:200), ACOX1 (ThermoFisher, PA5-82750, 1:200), catalase (Cell Signaling Technology, 12980, 1:800), anti-mouse IgG Alexa Fluor 647 (abcam, ab150115, 1:500), anti-rabbit IgG Alexa Fluor 488 (abcam, ab150077, 1:500). Lipid droplets were visualized by staining with 4,4-Difluoro-1,3,5,7,8-Pentamethyl-4-Bora-3a,4a-Diaza-s-Indacene (BODIPY) 493/505 (5 μM in PBS). The cells were stained with 4′,6-diamidino-2-phenylindole (DAPI) to visualize the nucleus. Following all staining, cells were imaged using a Zeiss 710 LSM confocal microscope.

Chemoenzymatic labeling

Elaboration with UDP-GalNAz:

O-GlcNAcylated proteins from cell lysates (150 μg) were labeled as previously described.[20] Briefly, proteins were precipitated by adding methanol (3x volume), chloroform (0.75x volume), and water (2.25x volume) followed by vortexing and centrifugation (21,2130 x g). The aqueous layer was removed and the pellet was washed with 2.5x volume of methanol 2-3 times. The pellet was dried and resolubilized with 40 μL dissolution buffer (20 mM HEPES, 1% SDS, pH 7.9). Water (49 μL), 5.5 mM MnCl (11 μL), and 80 μL 2.5x GalT labeling buffer (50 mM HEPES, 125 mM NaCl, 5% IGEPAL CA-630, pH 7.9) were added and the solution was vortexed. 10 μL of an engineered enzyme, GalT (Y289L, 2 mg/mL), and 10 μL of an artificial azido sugar, UDP-GalNAz (0.5 mM in 10 mM HEPES, pH 7.9, synthesized in house according to published procedures[51]), were added and the reaction was carried out at 4°C for 1 hour with end-over-end rotation. For proteins intended to undergo the SPACC reaction only, 10 μL of

iodoacetamide (Sigma Aldrich, 500 µM) was added and allowed to react for 1 hour at room temperature in the dark with end-over-end rotation. Control experiments were carried out in parallel in the absence of UDP-GalNAz. Following this, the proteins were precipitated as described above. Labeling of proteins from the GIT1 KD experiment were conducted on 100 µg of protein and half volumes were used for all steps.

CuAAC and SPAAC:

O-GlcNAcylated proteins were further elaborated with biotin or 5-kDa poly(ethylene) glycol (PEG) via either the CuAAC or strain-promoted azide-alkyne cycloaddition (SPAAC) reactions as described previously.[20] Briefly, for the CuAAC reaction, proteins were resolubilized in dissolution buffer (1% SDS in TBS pH 7.6) and in a separate tube, 300 µL H_2O, 7.5 µL BTTAA (10 mM, Click Chemistry Tools), 15 µL $CuSO_4$ (50 mM), and 15 µL of the biotin-PEG_4-alkyne (5 mM, Click Chemistry Tools) were added (quantities for 3 reactions). 100 µL of the mix was added to the redissolved protein, following which the solution was vortexed. 4 µL Tris(2-carboxyethyl)phosphine (100 mM, Sigma Aldrich) was then added to the reaction and the solution was allowed to react for 1 hour in the dark before being precipitated as before.

For the SPAAC reaction, proteins were resolubilized in dissolution buffer followed by addition of the desired dibenzocyclooctyne (DBCO). PEGylation (DBCO-mPEG, 5 kDa in DMSO, Click Chemistry Tools) took place at 95°C for 5 min using 1 mM DBCO-PEG. Biotinylaton (DBCO-biotin, 5 mM in DMSO) took place at room temperature for 1 hour in the dark with end-over-end rotation. Excess tag was removed by precipitation as before.

Enrichment of biotinylated proteins:

Proteins were resolubilized in dissolution buffer and incubated with streptavidin magnetic beads (ThermoFisher) for 1.5 hours in the dark. Beads were then washed 5 times with 0.5 ml of low salt buffer (100 mM Na_2HPO_4, 150 mM NaCl, 0.1% SDS, 1% Triton X-100, 0.5% sodium deoxycholate) and 5 times with 1 ml of high salt buffer (100 mM Na_2HPO_4, 500 mM NaCl, 0.2% Triton X-100). Biotinylated proteins were eluted by boiling the resin in 50 mM Tris-HCl pH 6.8, 2.5% SDS, 100 mM dithiothreitol (DTT), 10% glycerol, and 2 mM biotin for 15 min with occasional vortexing.

Quantification of O-GlcNAcylation

Following either reaction and, for biotinylated proteins, streptavidin capture, SDS-PAGE and Western blot for liprin-α1 were used to analyze O-GlcNAcylation. Western blot for the protein CREB [50] served as a positive control. For biotinylated proteins, the percentage of O-GlcNAcylated protein was calculated by taking the ratios of input and eluent weighted by proportion of the total protein in each lane as previously described.[52] For PEGylated proteins, the percentage of O-GlcNAcylated protein was calculated by dividing the intensity of the higher-MW shifted band to the total intensity of the protein in that lane also as previously described.[50]

Co-Immunoprecipitation

Neurons expressing OGT-FH containing HA and FLAG tags were grown and either silenced or KCl stimulated as described above. Cells were lysed after 26 days as previously described and diluted to 2 mg/mL with TBS buffer (1% Triton in TBS, Roche c0mplete protease inhibitor cocktail (Sigma Aldrich), TMG (0.1 mM), and phosphatase inhibitors (Cyclosporin A, okadaic acid, and a phosphatase inhibitor cocktail). The lysate was incubated with anti-FLAG magnetic beads (Sigma Aldrich) at 4°C overnight with end-over-end rotation. Some input lysate

was saved for Western Blotting. The beads were washed with 3 times with 0.1% Triton-X-100 in TBS pH 7.9 and eluted with 2% SDS in Tris, pH 8. Inputs and eluents were run on SDS-PAGE and Western blotted for HA (one of the tags on OGT), liprin-α1 and GIT1. Pulldown efficiency was calculated by measuring the intensity of the eluent bands relative to the input.

Fatty Acid Assay

Concentration of long-chain fatty acids (8 or more carbons) in Hep G2 cell lysates was determined using a Free Fatty Acid Quantitation Kit (Sigma Aldrich, MAK044). The cells were trypsinized and washed with PBS followed by lysis and fatty acid extraction per manufacturer's instructions, except that the fatty acids were left to dry in a fume hood overnight rather than vacuum dried. The colorimetric assay itself was performed per manufacturer's instructions.

Lentivirus production

HEK 293T cells were transfected with GIT1 shRNA (5' – GCCACCTTGATCATCGACATTC – 3', Sigma Aldrich) or scrambled shRNA (5' – AGTCCTTAGTCGAATCAGCCG – 3') lentiviral plasmids (Figure A.1), as well as lentiviral packaging plasmids (ViraPower Lentiviral Packaging Mix, ThermoFisher), using Lipofectamine 3000 (ThermoFisher) at 50-90% confluence according to manufacturer's instructions. The virus was harvested by collecting and replacing the media 24 and 48 hours post-transfection and concentrated using PEG precipitation.[42] The knockdown (KD) efficiency of the virus was

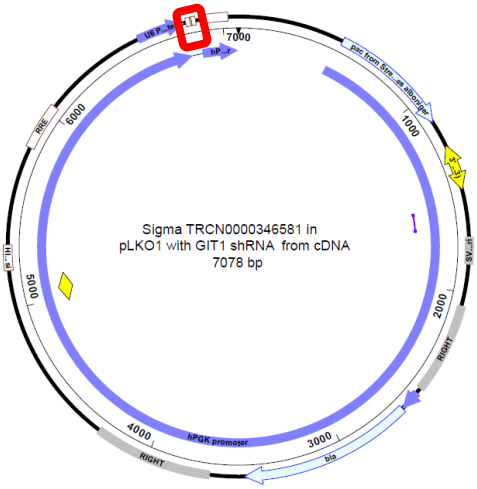

Figure A.1: Plasmid map of GIT1 shRNA vector. The red rectangle indicates the region containing the shRNA sequence for GIT1 KD:

validated by infecting primary mouse cortical neurons followed by lysis, SDS-PAGE, and Western blotting for GIT1.

Transfection

HEK 293T cells were grown on a Poly-D-Lysine (PDL) coated plate and treated at 50% confluency with siRNA for the protein of interest [BAP1 (Origene, SR322372)] or a scrambled sequence (Origene, SR30004) using MISSION siRNA transfection reagent and protocols (Sigma, S1452) to package the DNA for cellular uptake. Cells were incubated for 48 hours to allow sufficient time for the DNA to enter cells, after which their media was exchanged. Once sufficient time had passed for the siRNA machinery to KD the protein of interest (72 hours post-treatment), the cells were lysed as described above. Western Blots staining for the protein of interest with α-tubulin as a control were performed to evaluate KD efficiency.

Western blots and antibodies

The following primary antibodies were used for Western blotting (1:1000 dilution unless otherwise stated): anti-liprin-α1 (Proteintech, 14175-1-AP), anti-CREB (Cell Signaling Technology, 9104 (mouse), 4820 (rabbit)), anti-GIT1 (Cell Signaling Technology, sc-365084), anti-α-tubulin (Sigma Aldrich, T9026, 1:3000), anti-HA (Cell Signaling Technology, C29F4, 1:2000), anti-BAP1 (Cell Signaling Technology, A302-243A-M (1:1000), and 13187 (1:500)), anti-FOXK1 (Cell Signaling Technology, 12025S, 1:750), anti-FOXK2 (Cell Signaling Technology, 12008S), anti-FOXO3a (Cell Signaling Technology, 75D8), anti-SET1A (Cell Signaling Technology, 61702). The following secondary antibodies were used for Western blotting (1:10,000 dilution): anti-rabbit IgG Alexa Fluor Plus 680 (ThermoFisher, A27020), anti-

mouse IgG DyLight 800 (ThermoFisher, A11357). All Western blots were visualized and quantified using an Odyssey Infrared Imaging System and software (Li-Cor, Version 5.2).

Appendix B: Supplementary Data

Validation of 1 Hour GalT Incubation

The first step of the aforementioned chemoenzymatic labeling technique is labeling O-GlcNAcylated residues with an artificial UDP sugar using the engineered enzyme GalT.[20,53] Recent work in our laboratory has suggested that the reaction reaches completion in only 1 hour as opposed to overnight as previous reported.[20,53] To confirm this exciting new result, lysates from 293T cells were spiked with semisynthetic O-GlcNAcylated ubiquitin-HA[53] and chemoenzymatically labeled with 5 kDa PEG mass tags as described above except that the GalT labeling was left to proceed for either 1 hr or overnight (O/N). O-GlcNAcylation stoichiometry was then determined by Western blotting for CREB and HA. The results showed no significant difference in labeling between the 1 hour and O/N GalT incubations, indicating that the 1 hour incubation time can be used to expedite the overall labeling process (Figure B.1). Future experiments that utilize this technique will be carried out with the modified GalT incubation time.

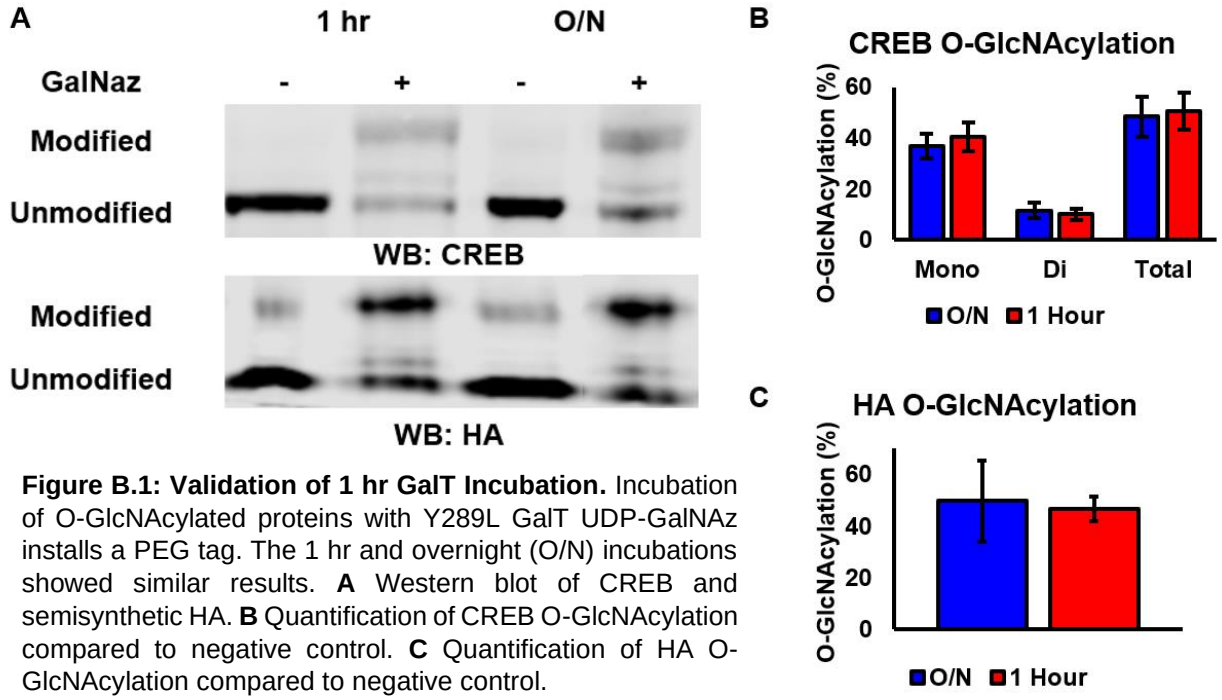

Figure B.1: Validation of 1 hr GalT Incubation. Incubation of O-GlcNAcylated proteins with Y289L GalT UDP-GalNAz installs a PEG tag. The 1 hr and overnight (O/N) incubations showed similar results. **A** Western blot of CREB and semisynthetic HA. **B** Quantification of CREB O-GlcNAcylation compared to negative control. **C** Quantification of HA O-GlcNAcylation compared to negative control.

Titration of GIT1 shRNA Lentivirus

Following production of the GIT1 shRNA lentivirus and scrambled control virus, KD efficacy and required dosage needed to be determined. To do this, neurons were prepared as described above in 12-well plates (1 mL well volume) and treated with 0 to 64 µL of GIT1 or scrambled virus after two weeks. Media was changed each day and cells were lysed 7 days post-infection. Western blot was conducted on the lysates to determine KD efficiency at each dosage (Figure B.2). Dosages were scaled to well volume for actual KD experiments.

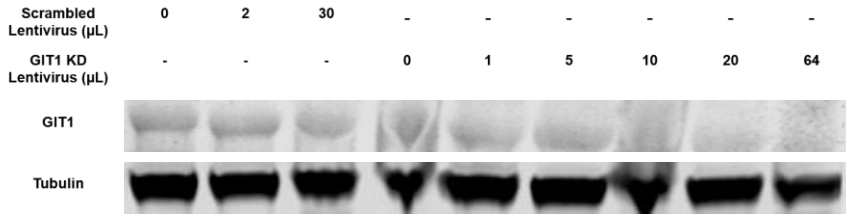

Figure B.2: GIT1 shRNA lentivirus titer. Primary mouse cortical neurons were transduced with lentivirus as indicated. A clear dose-response relationship was observed with a maximum KD efficiency

Appendix C: Image Processing Code

This code is partially adapted from:

v3_barcoding_meoh_fixed (2019) Katsuya Colón. Unpublished.

BE/Bi 103. Justin Bois, BE/Bi 103 GitHub. https://github.com/bebi103

```
#data compiling and processing
import glob
import numpy as np
import pandas as pd
import scipy
import os
import csv


# Image processing tools
import skimage
import skimage.io
import skimage.feature
import bebi103
import czifile


#plotting packages
import bokeh.io
#import bokeh_catplot
bokeh.io.output_notebook()
import holoviews as hv
hv.extension('bokeh')
import matplotlib.pyplot as plt
import seaborn as sns
import panel as pn
pn.extension()


#ignore warnings
import warnings
warnings.filterwarnings("ignore")
```

```
C:\Users\thism\anaconda3\lib\site-packages\bebi103\viz.py:37: UserWarning: DataShader import failed with error "cannot import nam
e 'encode_utf8' from 'bokeh.embed.notebook' (C:\Users\thism\anaconda3\lib\site-packages\bokeh\embed\notebook.py)".
Features requiring DataShader will not work and you will get exceptions.
  Features requiring DataShader will not work and you will get exceptions."""
```

Image Importing

```
def czi_to_numpy_array(im_names, im_dir):
    """
    Collects a list of im_names in im_dir into a numpy array.
```

```
    Inputs
        im_names: a list of the image file names to be converted
        im_dir: the path to the directory in which the images are stored. Must be a subdirectory of wherever the code is being ru
n

    Returns numpy array with all images as its elements

    Does not contain any error checking
    """
    # Initialize a list to load images into temporarily
    temp_arr = []

    # Add images to the list
    for im in im_names:
        # Compile the image
        im_czi = czifile.imread(im_dir + im)

        # Squeeze the image to get rid of empty dimensions
        squeezed_im = np.squeeze(im_czi)

        # Add the image to the array
        temp_arr.append(squeezed_im)

    # Convert the list into a numpy array
    numpy_arr = np.array(temp_arr)

    # Return the collected images
    return numpy_arr
# Get lists of image names
first_set_63x_dir = './First_Set_63x_Images/'
first_set_63x_names = os.listdir(first_set_63x_dir)

second_set_63x_dir = './Second_Set_63x_Images/'
second_set_63x_names = os.listdir(second_set_63x_dir)
# Check if the lists are correct
print("First set 63x names: ")
first_set_63x_names
First set 63x names:
['high_63x_snap_Avg8Speed7_SmallPinhole.czi',
 'high_TMG_63x_snap_Avg8Speed7_SmallPinhole.czi',
 'Low_63x_snap_Avg8Speed7_SmallPinhole.czi',
 'Low_TMG_63x_snap_Avg8Speed7_SmallPinhole.czi',
 'None_63x_snap_Avg8Speed7_SmallPinhole.czi']
print("Second set 63x names: ")
second_set_63x_names
Second set 63x names:
['HighTMG_63x_snap_Avg8Speed7_SmallPinhole.czi',
 'High_63x_snap_Avg8Speed7_SmallPinhole.czi',
```

```
 'LowTMG_63x_snap_Avg8Speed7_SmallPinhole.czi',
 'Low_63x_snap_Avg8Speed7_SmallPinhole.czi',
 'None_63x_snap_Avg8Speed7_SmallPinhole.czi']
# Collecting each list of images into a numpy array
first_set_63x_arr = czi_to_numpy_array(first_set_63x_names, first_set_63x_dir)

second_set_63x_arr = czi_to_numpy_array(second_set_63x_names, second_set_63x_dir)
# Check to make sure that each array contains the correct number of images
print("Dimensions of first set 63x array: ")
first_set_63x_arr.shape
Dimensions of first set 63x array:
(5, 3, 512, 512)
print("Dimensions of second set 63x array: ")
second_set_63x_arr.shape
Dimensions of second set 63x array:
(5, 3, 512, 512)
# Check to make sure that the different channels are different for the first image in each set
print("Same channels in first set 63x? ")
(first_set_63x_arr[0][0] == first_set_63x_arr[0][1]).all()
Same channels in first set 63x?
False
print("Same channels in second set 63x? ")
(second_set_63x_arr[0][0] == second_set_63x_arr[0][1]).all()
Same channels in second set 63x?
False
# Print out an example set of images to make sure everything worked correctly

# Print which image this is
print(first_set_63x_names[0] + '\n')

# DAPI channel:
print('DAPI Channel:')
bokeh.io.show(bebi103.image.imshow(first_set_63x_arr[0][0]))

# Lipid droplet channel:
print('Lipid droplet Channel:')
bokeh.io.show(bebi103.image.imshow(first_set_63x_arr[0][1]))

# Peroxisome channel:
print('Peroxisome Channel:')
bokeh.io.show(bebi103.image.imshow(first_set_63x_arr[0][2]))
high_63x_snap_Avg8Speed7_SmallPinhole.czi

DAPI Channel:
Lipid droplet Channel:
Peroxisome Channel:
# Get all of the snapshot .lsm file names for second set 100x images
second_set_100x_names = sorted(glob.glob('./Second_Set_100x_Images/*.lsm'))
```

```
# Check if the names are correct
second_set_100x_names
['./Second_Set_100x_Images\\HighTMG_100x_Pinhole_Avg16Speed7.lsm',
 './Second_Set_100x_Images\\High_100x_Pinhole_Avg16Speed7.lsm',
 './Second_Set_100x_Images\\LowTMG_100x_Pinhole_Avg16Speed7.lsm',
 './Second_Set_100x_Images\\Low_100x_Pinhole_Avg16Speed7.lsm',
 './Second_Set_100x_Images\\None_100x_Pinhole_Avg16Speed7.lsm']
# Compile the images from the 100x list into an image collection
second_set_100x_col = skimage.io.ImageCollection(second_set_100x_names, conserve_memory = True)

# Look at the shape of the collection to make sure the correct number of images are present
print("Dimensions of second set 100x collection: ")
second_set_100x_col[0].shape
Dimensions of second set 100x collection:
(512, 512, 3)
def im_col_to_grey(im_col):
    """
    Converts the first channel in each image in an image collection into greyscale
    Uses the skimage color.rgb2grey function

    Input
        im_col: a skimage image collection

    Returns a numpy array with all the images as its elements
    """
    # Initialize a list to load images into temporarily
    temp_arr = []

    # Add images to the list
    for im in im_col:
        # Convert channel of interest to grey scale
        grey_im = skimage.color.rgb2grey(im)

        # Add the image to the array
        temp_arr.append(grey_im)

    # Convert the list into a numpy array
    numpy_arr = np.array(temp_arr)

    # Return the collected images
    return numpy_arr
# Convert channel of interest (first channel) to grey scale
second_set_100x_arr = im_col_to_grey(second_set_100x_col)
# Look at the shape of the array to make sure the correct number of images are present still
print("Dimensions of second set 100x array: ")
second_set_100x_arr.shape
Dimensions of second set 100x array:
```

```
(5, 512, 512)
```

```
# Print out an example image to make sure everything worked correctly


# Print which image this is
print(second_set_100x_names[0] + '\n')


# Lipid droplet channel:
print('Lipid droplet Channel:')
bokeh.io.show(bebi103.image.imshow(second_set_100x_arr[0]))
```

```
./Second_Set_100x_Images\HighTMG_100x_Pinhole_Avg16Speed7.lsm


Lipid droplet Channel:
```

Image Segmentation

Zerocrossing Background Filter
This function finds edges of objects by finding the maximum rate of change in pixel intensity. First, a square structuring element is used to detect edges. Then the image is max/min filtered using this output. The sobel filter is then used to compute the rate of change. Finally, the edges are returned by comparing these values to the inputed threshold.

```
def zero_crossing_filter(im, selem, thresh):
    """
    Returns image with 1 if there is a zero crossing and 0 otherwise.

    thresh is the the minimal value of the gradient, as computed by Sobel
    filter, at crossing to count as a crossing.
    """

    # Do max filter and min filter
    im_max = scipy.ndimage.filters.maximum_filter(im, footprint=selem)
    im_min = scipy.ndimage.filters.minimum_filter(im, footprint=selem)

    # Compute gradients using Sobel filter
    im_grad = skimage.filters.sobel(im)

    # Return edges
    return (((im >= 0) & (im_min < 0)) | ((im <= 0) & (im_max > 0))) \
                & (im_grad >= thresh)
```

LoG Function
A gaussian filter is used to visualize the background, which is then subtracted from the image. The image is denoised using total variation denoiseing (tv_chambolle function). A laplacian of gaussian is then applied. The above zerocrossing function is used to segment the image. Following this, the image is skeletonized, holes are filled, and small objects (likely dust/noise) are removed before clear borders are defined.

```
def log(im, gauss_sigma, weight, log_sigma, selem, thresh, min_size, buffer_size):
    """
    A gaussian filter followed by a gaussian laplace filter is used to subtract background. The images are segmented using
    the zerocrossing filter function above. The shapes are then filled in and small objects are removed.
    """
```

```
    # Normalize image and convert to floats
    im_normalized = (im.astype(float) - im.min()) / (im.max() - im.min())

    # Use a filter to visualize background
    im_gauss = skimage.filters.gaussian(im_normalized, gauss_sigma)

    # Subtract the background
    im_subtracted = im_normalized - im_gauss

    # Denoise image
    im_denoised = skimage.restoration.denoise_tv_chambolle(im_subtracted, weight)

    # Apply laplacian of gaussian filter
    im_log = scipy.ndimage.filters.gaussian_laplace(im_denoised, log_sigma)

    # Apply zerocrossing filter function to detect edges
    im_edge = zero_crossing_filter(im_log, selem, thresh)

    # Skeletonize image
    im_skeletonized = skimage.morphology.skeletonize(im_edge)

    # Fill in holes
    im_filled = scipy.ndimage.morphology.binary_fill_holes(im_skeletonized)

    # Remove objects that are too small
    im_removed = skimage.morphology.remove_small_objects(im_filled, min_size = min_size)

    # Define a clear border for each object
    im_bordered = skimage.segmentation.clear_border(im_removed, buffer_size = buffer_size)

    # Return processed image
    return im_bordered
```

Processing images using the LoG and zerocrossing functions (1st 2 functions)

```
# Threshold and segment every image using previously optimized parameters and add to appropriate list
processed_list_first_set_63x = []
processed_list_second_set_63x = []
processed_list_second_set_100x = []

for im in first_set_63x_arr:
    im_thresh = log(
        im[1], gauss_sigma = 50.0, weight = 0.001, log_sigma = 1.5, selem = skimage.morphology.square(3),
        thresh = 0.001, min_size = 5, buffer_size = 5
    )
    processed_list_first_set_63x.append(im_thresh)

for im in second_set_63x_arr:
```

```
    im_thresh = log(
        im[1], gauss_sigma = 50.0, weight = 0.001, log_sigma = 1.5, selem = skimage.morphology.square(3),
        thresh = 0.001, min_size = 5, buffer_size = 5
    )
    processed_list_second_set_63x.append(im_thresh)

for im in second_set_100x_arr:
    im_thresh = log(
        im, gauss_sigma = 50.0, weight = 0.001, log_sigma = 1.5, selem = skimage.morphology.square(2),
        thresh = 0.001, min_size = 8, buffer_size = 5
    )
    processed_list_second_set_100x.append(im_thresh)
```

Thresholding images using the LoG_zerocrossing function (3rd function)
Viewing an example from each set

```
# Print which image this is
print(first_set_63x_names[0] + '\n')

# Print segmented images
print("LoG & Zerocrossing Segmented image: ")
bokeh.io.show(bebi103.image.imshow(processed_list_first_set_63x[0]))

# Comparing it to the original image
print("Original image: ")
bokeh.io.show(bebi103.image.imshow(first_set_63x_arr[0][1]))

# Print which image this is
print(second_set_63x_names[0] + '\n')

# Print segmented images
print("LoG & Zerocrossing Segmented image: ")
bokeh.io.show(bebi103.image.imshow(processed_list_second_set_63x[0]))

# Comparing it to the original image
print("Original image: ")
bokeh.io.show(bebi103.image.imshow(second_set_63x_arr[0][1]))

# Print which image this is
print(second_set_100x_names[0] + '\n')

# Print segmented images
print("LoG & Zerocrossing Segmented image: ")
bokeh.io.show(bebi103.image.imshow(processed_list_second_set_100x[0]))

# Comparing it to the original image
print("Original image: ")
bokeh.io.show(bebi103.image.imshow(second_set_100x_arr[0]))
high_63x_snap_Avg8Speed7_SmallPinhole.czi
```

```
LoG & Zerocrossing Segmented image:
Original image:
HighTMG_63x_snap_Avg8Speed7_SmallPinhole.czi

LoG & Zerocrossing Segmented image:
Original image:
./Second_Set_100x_Images\HighTMG_100x_Pinhole_Avg16Speed7.lsm

LoG & Zerocrossing Segmented image:
Original image:
```

Image Statistics

```
# Label all binary images
labels_list_first_set_63x = []
labels_list_second_set_63x = []
labels_list_second_set_100x = []

for i in processed_list_first_set_63x:
    im_labeled, n_labels = skimage.measure.label(i, background=0, return_num=True)
    labels_list_first_set_63x.append((im_labeled, n_labels))

for i in processed_list_second_set_63x:
    im_labeled, n_labels = skimage.measure.label(i, background=0, return_num=True)
    labels_list_second_set_63x.append((im_labeled, n_labels))

for i in processed_list_second_set_100x:
    im_labeled, n_labels = skimage.measure.label(i, background=0, return_num=True)
    labels_list_second_set_100x.append((im_labeled, n_labels))
# Check that lebels worked correctly by looking at one of the labeled images
labels_list_first_set_63x[0]
(array([[0, 0, 0, ..., 0, 0, 0],
        [0, 0, 0, ..., 0, 0, 0],
        [0, 0, 0, ..., 0, 0, 0],
        ...,
        [0, 0, 0, ..., 0, 0, 0],
        [0, 0, 0, ..., 0, 0, 0],
        [0, 0, 0, ..., 0, 0, 0]], dtype=int64),
 154)
# Show number of cells
print("Number of individual cells = ", labels_list_first_set_63x[0][1])

# See result
bokeh.io.show(
    bebi103.image.imshow(
        labels_list_first_set_63x[0][0]
    )
```

```
)
Number of individual cells =  154
# Get properties from the lipid droplet channel for all images
im_props_list_first_set_63x = []
im_props_list_second_set_63x = []
im_props_list_second_set_100x = []

for i in range(0,len(labels_list_first_set_63x)):
    im_props = skimage.measure.regionprops(labels_list_first_set_63x[i][0], intensity_image = first_set_63x_arr[i][1])
    im_props_list_first_set_63x.append((im_props, first_set_63x_names[i]))

for i in range(0,len(labels_list_second_set_63x)):
    im_props = skimage.measure.regionprops(labels_list_second_set_63x[i][0], intensity_image = second_set_63x_arr[i][1])
    im_props_list_second_set_63x.append((im_props, second_set_63x_names[i]))

for i in range(0,len(labels_list_second_set_100x)):
    im_props = skimage.measure.regionprops(labels_list_second_set_100x[i][0], intensity_image = second_set_100x_arr[i])
    im_props_list_second_set_100x.append((im_props, second_set_100x_names[i]))
# Total number of lipid droplets
tot_droplets_first_set_63x = []
tot_droplets_second_set_63x = []
tot_droplets_second_set_100x = []

for label in labels_list_first_set_63x:
    tot_droplets_first_set_63x.append(label[1])

for label in labels_list_second_set_63x:
    tot_droplets_second_set_63x.append(label[1])

for label in labels_list_second_set_100x:
    tot_droplets_second_set_100x.append(label[1])
# Test that one of the total numbers lists look correct
tot_droplets_first_set_63x
[154, 99, 203, 115, 116]
# Combining all the numbers of lipid droplets per image into a list
data = []
data.append(["First Set 63x:", 0])
for i in range(0, len(first_set_63x_names)):
    data.append([first_set_63x_names[i], tot_droplets_first_set_63x[i]])

data.append(["Second Set 63x:", 0])
for i in range(0, len(second_set_63x_names)):
    data.append([second_set_63x_names[i], tot_droplets_second_set_63x[i]])

data.append(["Second Set 100x:", 0])
for i in range(0, len(second_set_100x_names)):
    data.append([second_set_100x_names[i], tot_droplets_second_set_100x[i]])
```

```
df = pd.DataFrame(
    data = data, columns = ["Image Name", "Number of Lipid Droplets"]
)

# View chart
df
```

First Set 63x

```
# Areas of lipid droplets in oixels
data = [[prop.area, im_props_list_first_set_63x[i][1]]
        for i in range(0,len(im_props_list_first_set_63x)) for prop in im_props_list_first_set_63x[i][0]]

df_area = pd.DataFrame(
    data = data, columns = ["Lipid Droplet Area (pixels)", "Image Name"]
)

df_area
```

```
# Write the raw data to a .csv file to save it
with open('First_set_63x.csv', 'w', newline='') as csvfile:
    writer = csv.writer(csvfile)
    writer.writerow(["Lipid droplet area (pixels)"] + ["Filename"])
    writer.writerows(df_area.values)
# Average area of lipid droplets
area = df_area.groupby("Image Name")

area_mean = area.mean()

print("Mean Areas: ")
area_mean
Mean Areas:
```

```
# Standard deviation of lipid droplet areas
area_stdev = area.std()

print("Standard Deviation of Areas: ")
area_stdev
Standard Deviation of Areas:
```

```
#violin plots with jitter box

violin = hv.Violin(df_area, vdims="Lipid Droplet Area (pixels)", kdims = "Image Name")
violin.opts(xrotation = 90, xlabel = "", inner='quartiles', cut=0.2, bandwidth=0.4,
            padding = 0.1, violin_fill_color = "lightgrey",
            frame_height = 400, frame_width = 300)
```

```
jitter_box = hv.Scatter(df_area, vdims="Lipid Droplet Area (pixels)", kdims = "Image Name")
jitter_box.opts(jitter=0.3, alpha=0.4, size=5, height=600, width=600, color = "k")

violin*jitter_box
#box plots with jitter box

box = hv.BoxWhisker(df_area, vdims="Lipid Droplet Area (pixels)", kdims = "Image Name")
box.opts(xrotation = 90, xlabel = "",box_fill_color = "lightgrey", padding = 0.1, outlier_alpha = 0,
            frame_height = 400, frame_width = 300)

jitter_box = hv.Scatter(df_area, vdims="Lipid Droplet Area (pixels)", kdims = "Image Name")
jitter_box.opts(jitter=0.3, alpha=0.4, size=5, height=600, width=600, color = "k")

box*jitter_box
```

Second Set 63x

```
# Areas of lipid droplets in oixels
data = [[prop.area, im_props_list_second_set_63x[i][1]]
        for i in range(0,len(im_props_list_second_set_63x)) for prop in im_props_list_second_set_63x[i][0]]

df_area = pd.DataFrame(
    data = data, columns = ["Lipid Droplet Area (pixels)", "Image Name"]
)

df_area
```

```
# Write the raw data to a .csv file to save it
with open('Second_set_63x.csv', 'w', newline='') as csvfile:
    writer = csv.writer(csvfile)
    writer.writerow(["Lipid droplet area (pixels)"] + ["Filename"])
    writer.writerows(df_area.values)
# Average area of lipid droplets
area = df_area.groupby("Image Name")

area_mean = area.mean()

print("Mean Areas: ")
area_mean
Mean Areas:
```

```
# Standard deviation of lipid droplet areas
area_stdev = area.std()

print("Standard Deviation of Areas: ")
area_stdev
Standard Deviation of Areas:
```

```
#violin plots with jitter box

violin = hv.Violin(df_area, vdims="Lipid Droplet Area (pixels)", kdims = "Image Name")
violin.opts(xrotation = 90, xlabel = "", inner='quartiles', cut=0.2, bandwidth=0.4,
            padding = 0.1, violin_fill_color = "lightgrey",
            frame_height = 400, frame_width = 300)

jitter_box = hv.Scatter(df_area, vdims="Lipid Droplet Area (pixels)", kdims = "Image Name")
jitter_box.opts(jitter=0.3, alpha=0.4, size=5, height=600, width=600, color = "k")

violin*jitter_box
#box plots with jitter box

box = hv.BoxWhisker(df_area, vdims="Lipid Droplet Area (pixels)", kdims = "Image Name")
box.opts(xrotation = 90, xlabel = "",box_fill_color = "lightgrey", padding = 0.1, outlier_alpha = 0,
            frame_height = 400, frame_width = 300)

jitter_box = hv.Scatter(df_area, vdims="Lipid Droplet Area (pixels)", kdims = "Image Name")
jitter_box.opts(jitter=0.3, alpha=0.4, size=5, height=600, width=600, color = "k")

box*jitter_box
```

Second Set 100x

```
# Areas of lipid droplets in oixels
data = [[prop.area, im_props_list_second_set_100x[i][1]]
        for i in range(0,len(im_props_list_second_set_100x)) for prop in im_props_list_second_set_100x[i][0]]

df_area = pd.DataFrame(
    data = data, columns = ["Lipid Droplet Area (pixels)", "Image Name"]
)

df_area
```

```
# Write the raw data to a .csv file to save it
with open('Second_set_100x.csv', 'w', newline='') as csvfile:
    writer = csv.writer(csvfile)
    writer.writerow(["Lipid droplet area (pixels)"] + ["Filename"])
    writer.writerows(df_area.values)
# Average area of lipid droplets
area = df_area.groupby("Image Name")

area_mean = area.mean()

print("Mean Areas: ")
area_mean
```

```
Mean Areas:
```

```
# Standard deviation of lipid droplet areas
area_stdev = area.std()

print("Standard Deviation of Areas: ")
area_stdev
Standard Deviation of Areas:
```

```
#violin plots with jitter box

violin = hv.Violin(df_area, vdims="Lipid Droplet Area (pixels)", kdims = "Image Name")
violin.opts(xrotation = 90, xlabel = "", inner='quartiles', cut=0.2, bandwidth=0.4,
            padding = 0.1, violin_fill_color = "lightgrey",
            frame_height = 400, frame_width = 300)

jitter_box = hv.Scatter(df_area, vdims="Lipid Droplet Area (pixels)", kdims = "Image Name")
jitter_box.opts(jitter=0.3, alpha=0.4, size=5, height=600, width=600, color = "k")

violin*jitter_box
#box plots with jitter box

box = hv.BoxWhisker(df_area, vdims="Lipid Droplet Area (pixels)", kdims = "Image Name")
box.opts(xrotation = 90, xlabel = "",box_fill_color = "lightgrey", padding = 0.1, outlier_alpha = 0,
            frame_height = 400, frame_width = 300)

jitter_box = hv.Scatter(df_area, vdims="Lipid Droplet Area (pixels)", kdims = "Image Name")
jitter_box.opts(jitter=0.3, alpha=0.4, size=5, height=600, width=600, color = "k")

box*jitter_box
```

Bibliography

(1) Vaidyanathan, K.; Wells, L. Multiple Tissue-Specific Roles for the O-GlcNAc Post-Translational Modification in the Induction of and Complications Arising from Type II Diabetes. *Journal of Biological Chemistry*. American Society for Biochemistry and Molecular Biology Inc. December 12, 2014, pp 34466–34471. https://doi.org/10.1074/jbc.R114.591560.

(2) Ruan, H.-B.; Singh, J. P.; Li, M.-D.; Wu, J.; Yang, X. Cracking the O-GlcNAc Code in Metabolism. *Trends Endocrinol. Metab.* **2013**, *24* (6), 301–309. https://doi.org/10.1016/J.TEM.2013.02.002.

(3) Alzheimer Association science staff. 2018 Alzheimer's Disease Facts and Figures. *Alzheimer's Dement.* **2018**, *14* (3), 367–429. https://doi.org/10.1016/J.JALZ.2018.02.001.

(4) Yuzwa, S. A.; Vocadlo, D. J. O -GlcNAc and Neurodegeneration : Biochemical Mechanisms and Potential Roles in Alzheimer ' s Disease and beyond. *Chem Soc Rev* **2014**, *43*, 6839–6858. https://doi.org/10.1039/C4CS00038B.

(5) Baldini, S. F.; Wavelet, C.; Hainault, I.; Guinez, C.; Lefebvre, T. The Nutrient-Dependent O-GlcNAc Modification Controls the Expression of Liver Fatty Acid Synthase. *J. Mol. Biol.* **2016**, *428* (16), 3295–3304. https://doi.org/10.1016/J.JMB.2016.04.035.

(6) Baes, M.; Van Veldhoven, P. P. Hepatic Dysfunction in Peroxisomal Disorders. *Biochim. Biophys. Acta - Mol. Cell Res.* **2016**, *1863* (5), 956–970. https://doi.org/10.1016/J.BBAMCR.2015.09.035.

(7) Tansey, J. T.; Sztalryd, C.; Hlavin, E. M.; Kimmel, A. R.; Londos, C. The Central Role of Perilipin A in Lipid Metabolism and Adipocyte Lipolysis. *IUBMB Life*. July 2004, pp 379–385. https://doi.org/10.1080/15216540400009968.

(8) Issad, T.; Kuo, M. O-GlcNAc Modification of Transcription Factors, Glucose Sensing and Glucotoxicity. *Trends Endocrinol. Metab.* **2008**, *19* (10), 380–389. https://doi.org/10.1016/J.TEM.2008.09.001.

(9) Anthonisen, E. H.; Berven, L.; Holm, S.; Nygård, M.; Nebb, H. I.; Grønning-Wang, L. M. Nuclear Receptor Liver X Receptor Is O-GlcNAc-Modified in Response to Glucose. *J. Biol. Chem.* **2010**, *285* (3), 1607–1615. https://doi.org/10.1074/jbc.M109.082685.

(10) Ruan, H. Bin; Ma, Y.; Torres, S.; Zhang, B.; Feriod, C.; Heck, R. M.; Qian, K.; Fu, M.; Li, X.; Nathanson, M. H.; et al. Calcium-Dependent O-GlcNAc Signaling Drives Liver Autophagy in Adaptation to Starvation. *Genes Dev.* **2017**, *31* (16), 1655–1665. https://doi.org/10.1101/gad.305441.117.

(11) Hart, G. W.; Slawson, C.; Ramirez-Correa, G.; Lagerlof, O. Cross Talk Between O-GlcNAcylation and Phosphorylation: Roles in Signaling, Transcription, and Chronic Disease. *Annu. Rev. Biochem.* **2011**, *80* (1), 825–858. https://doi.org/10.1146/annurev-biochem-060608-102511.

(12) Yang, X.; Qian, K. Protein O-GlcNAcylation: Emerging Mechanisms and Functions. *Nat. Rev. Mol. Cell Biol.* **2017**, 452–465. https://doi.org/10.1038/nrm.2017.22.

(13) Lefebvre, T.; Dehennaut, V.; Guinez, C.; Olivier, S.; Drougat, L.; Mir, A. M.; Mortuaire, M.; Vercoutter-Edouart, A. S.; Michalski, J. C. Dysregulation of the Nutrient/Stress Sensor O-GlcNAcylation Is Involved in the Etiology of Cardiovascular Disorders, Type-2 Diabetes and Alzheimer's Disease. *Biochim. Biophys. Acta - Gen. Subj.* **2010**, *1800* (2), 67–79. https://doi.org/10.1016/j.bbagen.2009.08.008.

(14) Shafi, R.; Iyer, S. P.; Ellies, L. G.; O'Donnell, N.; Marek, K. W.; Chui, D.; Hart, G. W.; Marth, J. D. The O-GlcNAc Transferase Gene Resides on the X Chromosome and Is Essential for Embryonic Stem Cell Viability and Mouse Ontogeny. *Proc. Natl. Acad. Sci. U. S. A.* **2000**, *97* (11), 5735–5739. https://doi.org/10.1073/pnas.100471497.

(15) Lefebvre, T.; Issad, T. 30 Years Old: O-GlcNAc Reaches the Age of Reason - Regulation of Cell Signaling and Metabolism by O-GlcNAcylation. *Front. Endocrinol. (Lausanne).* **2015**, *6* (17), 1–2. https://doi.org/10.3389/fendo.2015.00017.

(16) Wells, L.; Vosseller, K.; Hart, G. W. A Role for N-Acetylglucosamine as a Nutrient Sensor and Mediator of Insulin Resistance. *Cell. Mol. Life Sci.* **2003**, *60* (2), 222–228. https://doi.org/10.1007/s000180300017.

(17) Alonso, J.; Schimpl, M.; Van Aalten, D. M. F. O-GlcNAcase: Promiscuous Hexosaminidase or Key Regulator of O-GlcNAc Signaling? *Journal of Biological Chemistry*. 2014. https://doi.org/10.1074/jbc.R114.609198.

(18) Banerjee, P. S.; Lagerlöf, O.; Hart, G. W. Roles of O-GlcNAc in Chronic Diseases of Aging. *Mol. Aspects Med.* **2016**. https://doi.org/10.1016/j.mam.2016.05.005.

(19) John W. Thompson,* Matthew E. Griffin,* Yao Xiao,* Michael J. Sweredoski, Rita B. Aksenfeld, Elizabeth H. Jensen, Yelena Koldobskaya, Andrew L. Schacht, Terry D. Kim, Priya Choudhry, Annie Moradian, Brett Lomenick, Spiros D. Garbis, L. C. H.-W. Functional Glycoproteomics by Integrated Network Assembly and Partitioning.

(20) Thompson, J. W.; Griffin, M. E.; Hsieh-wilson, L. C. Methods for the Detection , Study , and Dynamic Profiling of O-GlcNAc Glycosylation. *Methods Enzymol.* **2017**, *598*, 101–135. https://doi.org/10.1016/bs.mie.2017.06.009.

(21) Cline, M. S.; Smoot, M.; Cerami, E.; Kuchinsky, A.; Landys, N.; Workman, C.; Christmas, R.; Avila-Campilo, I.; Creech, M.; Gross, B.; et al. Integration of Biological Networks and Gene Expression Data Using Cytoscape. *Nat. Protoc.* **2007**, *2* (10), 2366–2382. https://doi.org/10.1038/nprot.2007.324.

(22) Su, G.; Kuchinsky, A.; Morris, J. H.; States, D. J.; Meng, F. GLay: Community Structure Analysis of Biological Networks. *BIOINFORMATICS* **2010**, *26* (24), 3135–3137. https://doi.org/10.1093/bioinformatics/btq596.

(23) Scheuermann, J. C.; De Ayala Alonso, A. G.; Oktaba, K.; Ly-Hartig, N.; McGinty, R. K.; Fraterman, S.; Wilm, M.; Muir, T. W.; Müller, J. Histone H2A Deubiquitinase Activity of the Polycomb Repressive Complex PR-DUB. *Nature* **2010**, *465* (7295), 243–247. https://doi.org/10.1038/nature08966.

(24) Hauri, S.; Comoglio, F.; Seimiya, M.; Gerstung, M.; Glatter, T.; Hansen, K.; Aebersold, R.; Paro, R.; Gstaiger, M.; Beisel, C. A High-Density Map for Navigating the Human Polycomb Complexome. *Cell Rep.* **2016**, *17* (2), 583–595. https://doi.org/10.1016/j.celrep.2016.08.096.

(25) Cai, Y.; Jin, J.; Swanson, S. K.; Cole, M. D.; Choi, S. H.; Florens, L.; Washburn, M. P.; Conaway, J. W.; Conaway, R. C. Subunit Composition and Substrate Specificity of a MOF-Containing Histone Acetyltransferase Distinct from the Male-Specific Lethal (MSL) Complex. *J. Biol. Chem.* **2010**, *285* (7), 4268–4272. https://doi.org/10.1074/jbc.C109.087981.

(26) Migliori, V.; Mapelli, M.; Guccione, E. On WD40 Proteins Propelling Our Knowledge of Transcriptional Control? *Epigenetics* **2012**, *7* (8), 815–822. https://doi.org/10.4161/epi.21140.

(27) Luo, Z.; Lin, C.; Shilatifard, A. The Super Elongation Complex (SEC) Family in Transcriptional Control. *Nature Reviews Molecular Cell Biology*. September 2012, pp 543–547. https://doi.org/10.1038/nrm3417.

(28) Jeronimo, C.; Forget, D.; Bouchard, A.; Li, Q.; Chua, G.; Poitras, C.; Thérien, C.; Bergeron, D.; Bourassa, S.; Greenblatt, J.; et al. Systematic Analysis of the Protein Interaction Network for the Human Transcription Machinery Reveals the Identity of the 7SK Capping Enzyme. *Mol. Cell* **2007**, *27* (2), 262–274. https://doi.org/10.1016/j.molcel.2007.06.027.

(29) Simone, C.; Stiegler, P.; Bagella, L.; Pucci, B.; Bellan, C.; De Falco, G.; De Luca, A.; Guanti, G.; Puri, P. L.; Giordano, A. Activation of MyoD-Dependent Transcription by Cdk9/Cyclin T2. *Oncogene* **2002**, *21*, 4137–4148. https://doi.org/10.1038/sj.onc.

(30) Ko, J.; Kim, S.; Valtschanoff, J. G.; Shin, H.; Lee, J.; Sheng, M.; Premont, R. T.; Weinberg, R. J.; Kim, E. Interaction between Liprin- α and GIT1 Is Required for AMPA Receptor Targeting. **2003**, *23* (5), 1667–1677.

(31) Kaur, N.; Reumann, S.; Hu, J. Peroxisome Biogenesis and Function. *Arab. B.* **2009**, *7*. https://doi.org/10.1199/tab.0123.

(32) John W. Thompson,* Matthew E. Griffin,* Michael J. Sweredoski, Rita B. Aksenfeld, Daniel E. Mason, Annie Moradrian, Eric C. Peters, L. C. H.-W. Quantitative Functional Glycoproteomics Reveals Widespread Changes in the Db/Db Mouse Liver.

(33) Gao, Q.; Goodman, J. The Lipid Droplet—a Well-Connected Organelle. *Front. Cell Dev. Biol.* **2015**, *3*, 49.

(34) Yang, Y.; Fu, M.; Li, M.-D.; Zhang, K.; Zhang, B.; Wang, S.; Liu, Y.; Ni, W.; Ong, Q.; Mi, J.; et al. O-GlcNAc Transferase Inhibits Visceral Fat Lipolysis and Promotes Diet-Induced Obesity. *Nat. Commun.* **2020**, *11* (1), 181. https://doi.org/10.1038/s41467-019-13914-8.

(35) Xu, S.; Zou, F.; Diao, Z.; Zhang, S.; Deng, Y.; Zhu, X.; Cui, L.; Yu, J.; Zhang, Z.; Bamigbade, A. T.; et al. Perilipin 2 and Lipid Droplets Provide Reciprocal Stabilization. *Biophys. Reports* **2019**, *5* (3), 145–160. https://doi.org/10.1007/s41048-019-0091-5.

(36) Itabe, H.; Yamaguchi, T.; Nimura, S.; Sasabe, N. Perilipins: A Diversity of Intracellular Lipid Droplet Proteins. *Lipids in Health and Disease*. BioMed Central Ltd. April 28, 2017. https://doi.org/10.1186/s12944-017-0473-y.

(37) Ruan, H. Bin; Han, X.; Li, M. D.; Singh, J. P.; Qian, K.; Azarhoush, S.; Zhao, L.; Bennett, A. M.; Samuel, V. T.; Wu, J.; et al. O-GlcNAc Transferase/Host Cell Factor C1 Complex Regulates Gluconeogenesis by Modulating PGC-1α Stability. *Cell Metab.* **2012**, *16* (2), 226–237. https://doi.org/10.1016/j.cmet.2012.07.006.

(38) Olson, C. M.; Jiang, B.; Erb, M. A.; Liang, Y.; Doctor, Z. M.; Zhang, Z.; Zhang, T.; Kwiatkowski, N.; Boukhali, M.; Green, J. L.; et al. Pharmacological Perturbation of CDK9 Using Selective CDK9 Inhibition or Degradation. *Nat. Chem. Biol.* **2018**, *14* (2), 163–170. https://doi.org/10.1038/nchembio.2538.

(39) Wyszynski, M.; Kim, E.; Dunah, A. W.; Passafaro, M.; Valtschanoff, J. G.; Serra-page, C.; Streuli, M.; Weinberg, R. J.; Sheng, M.; Hill, C.; et al. Interaction between GRIP and Liprin- α / SYD2 Is Required for AMPA Receptor Targeting. *Neuron* **2002**, *34*, 39–52.

(40) Shepherd, J. D.; Huganir, R. L. The Cell Biology of Synaptic Plasticity : AMPA Receptor Trafficking. *Annu. Rev. Cell Dev. Biol. 2007.* **2007**, No. 23, 613–643. https://doi.org/10.1146/annurev.cellbio.23.090506.123516.

(41) Im, Y. J.; Park, S. H.; Rho, S.; Lee, J. H.; Kang, G. B.; Sheng, M.; Kim, E.; Eom, S. H. Crystal Structure of GRIP1 PDZ6-Peptide Complex Reveals the Structural Basis for Class II PDZ Target Recognition and PDZ Domain-Mediated Multimerization *. *J Biol Chem.* **2003**, *278* (10), 8501–8507. https://doi.org/10.1074/jbc.M212263200.

(42) Kutner, R. H.; Zhang, X. Y.; Reiser, J. Production, Concentration and Titration of Pseudotyped HIV-1-Based Lentiviral Vectors. *Nat. Protoc.* **2009**. https://doi.org/10.1038/nprot.2009.22.

(43) Zhang, K.; Yin, R.; Yang, X. O-GlcNAc: A Bittersweet Switch in Liver. *Front. Endocrinol. (Lausanne).* **2014**, *5*, 221. https://doi.org/10.3389/fendo.2014.00221.

(44) Ji, S.; Park, S. Y.; Roth, J.; Kim, H. S.; Cho, J. W. O-GlcNAc Modification of PPARγ Reduces Its Transcriptional Activity. *Biochem. Biophys. Res. Commun.* **2012**, *417* (4), 1158–1163. https://doi.org/https://doi.org/10.1016/j.bbrc.2011.12.086.

(45) Naganuma, T.; Kihara, A. Two Modes of Regulation of the Fatty Acid Elongase ELOVL6 by the 3-Ketoacyl-CoA Reductase KAR in the Fatty Acid Elongation Cycle. *PLoS One* **2014**, *9* (7), e101823–e101823. https://doi.org/10.1371/journal.pone.0101823.

(46) Matsuzaka, T.; Kuba, M.; Koyasu, S.; Yamamoto, Y.; Motomura, K.; Arulmozhiraja, S.; Ohno, H.; Sharma, R.; Shimura, T.; Okajima, Y.; et al. Hepatocyte ELOVL Fatty Acid Elongase 6 Determines Ceramide Acyl-Chain Length and Hepatic Insulin Sensitivity in Mice. *Hepatology* **2020**, *71* (5), 1609–1625. https://doi.org/10.1002/hep.30953.

(47) Yang, X.; Ongusaha, P. P.; Miles, P. D.; Havstad, J. C.; Zhang, F.; So, W. V.; Kudlow, J. E.; Michell, R. H.; Olefsky, J. M.; Field, S. J.; et al. Phosphoinositide Signalling Links O-GlcNAc Transferase to Insulin Resistance. *Nature* **2008**, *451* (7181), 964–969. https://doi.org/10.1038/nature06668.

(48) Tan, E. P.; McGreal, S. R.; Graw, S.; Tessman, R.; Koppel, S. J.; Dhakal, P.; Zhang, Z.; Machacek, M.; Zachara, N. E.; Koestler, D. C.; et al. Sustained O-GlcNAcylation Reprograms Mitochondrial Function to Regulate Energy Metabolism. *J. Biol. Chem.* **2017**, *292* (36), 14940–14962. https://doi.org/10.1074/jbc.M117.797944.

(49) Yuzwa, S. A.; Macauley, M. S.; Heinonen, J. E.; Shan, X.; Dennis, R. J.; He, Y.; Whitworth, G. E.; Stubbs, K. A.; McEachern, E. J.; Davies, G. J.; et al. A Potent Mechanism-Inspired O-GlcNAcase Inhibitor That Blocks Phosphorylation of Tau in Vivo. *Nat. Chem. Biol.* **2008**, *4* (8), 483–490. https://doi.org/10.1038/nchembio.96.

(50) Rexach, J. E.; Clark, P. M.; Mason, D. E.; Neve, R. L.; Eric, C.; Hsieh-wilson, L. C. Dynamic O-GlcNAc Modification Regulates CREB-Mediated Gene Expression and Memory Formation. *Nat Chem Biol.* **2012**, *8* (3), 253–261. https://doi.org/10.1038/nchembio.770.Dynamic.

(51) Hang, H. C.; Yu, C.; Kato, D. L.; Bertozzi, C. R. Animal Cell Mutants Defective in Glycosaminoglycan Biosynthesis. *PNAS* **2003**, *82* (10), 3197–3201. https://doi.org/10.1073/pnas.82.10.3197.

(52) Yi, W. Y.; Clark, P. M.; Mason, D. E.; Keenan, M. C.; Hill, C.; Goddard III, W. A.; Peters, E. C.; Driggers, E. M.; Hsieh-Wilson, L. C. Phosphofructokinase 1 Glycosylation Regulates Cell Growth and Metabolism. *Science (80-.).* **2012**, *337*, 975–980. https://doi.org/10.1126/science.1225237.

(53) Darabedian, N.; Thompson, J. W.; Chuh, K. N.; Hsieh-Wilson, L. C.; Pratt, M. R. Optimization of Chemoenzymatic Mass Tagging by Strain-Promoted Cycloaddition (SPAAC) for the Determination of O-GlcNAc Stoichiometry by Western Blotting. *Biochemistry* **2018**, *57* (40), 5769–5774.

https://doi.org/10.1021/acs.biochem.8b00648.